SHALLOW CUMULUS CONVECTION

A. P. SIEBESMA
Royal Netherlands Meteorological Institute (KNMI)
Postbox 201, 3730 AE De Bilt, The Netherlands

1. Introduction

Shallow cumulus convection plays a crucial role in determining the vertical thermodynamic structure of the atmosphere and influences the large-scale circulation significantly in both tropics and mid-latitudes. This is most clearly demonstrated in the Hadley circulation over the tropical oceans, such as schematically illustrated in Fig. 1. In the subtropical belts, the surface evaporation from the ocean increases significantly due to the enhanced vertical transport of heat and moisture by shallow cumulus clouds, which are usually referred to as trade-wind cumuli. This enhanced moisture, collected in the trade-wind boundary layer, is transported by the trade winds towards the intertropical convergence zone (ITCZ), where it is finally released as latent heat in deep convective precipitating cumulus towers. Since this latent heat release is an important engine of the Hadley circulation, the enhanced surface evaporation upstream in the trade-wind region can be regarded as a fuel supply for this circulation. It is in this context that the presence of shallow cumuli, though small in individual size and non-precipitating, intensifies the large-scale circulation. Locally, the vertical transport of heat and moisture by the shallow cumulus clouds is also important to counteract the drying and warming effects of the large-scale subsidence induced by the Hadley circulation. As a result, a steady thermodynamic state of the vertical structure of the trade-wind region can be maintained.

As already suggested by the title we will limit ourselves to *shallow* cumulus convection of clouds whose vertical extent is small enough to be non-precipitative. Therefore the word "shallow" should be interpreted as "non-precipitative". Consequently we will not touch upon any microphysical issues dealing with transitions of liquid water to ice and precipitation and the interaction of precipitation with the dynamics. It is exactly the feedback of the microphysics through the precipitation with the dynamics

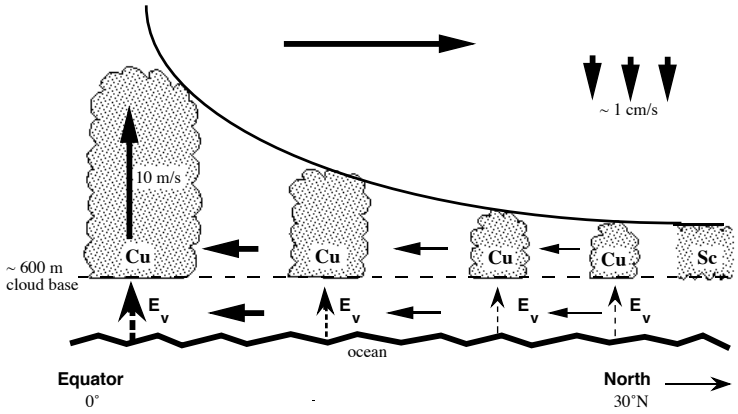

Figure 1. Schematic cross-section of one branch of the Hadley circulation, illustrating the enhancement of moisture convergence in the ITCZ due to the presence of trade-wind cumuli upstream (After Tiedtke[60]).

which makes precipitative *deep* cumulus convection fundamentally different and more complicated than non-precipitative *shallow* cumulus convection.

Main emphasis in this paper is placed on the vertical transport of moisture and heat. It turns out that the mixing of cumulus clouds with the environment is a key issue, both for the fundamental understanding and the more practical issue of parameterization of vertical transport by shallow cumulus convection. Although we are dealing with a relatively simple case of non-precipitative convection we shall see that the theoretical understanding of these mixing processes is still in a rather primitive state. This makes shallow cumulus convection such a challenging topic; while being the most simplest form of cumulus dynamics, apparently it is highly non-trivial and still awaiting better theoretical understanding.

The organization of this paper is as follows. As a prerequisite for the non-expert we give in section 2 a short overview of the essentials of thermodynamics for moist air. Section 3 reviews our current knowledge of *individual* shallow cumuli and their mixing with the environment. Section 4 deals with the dynamics of a cumulus ensemble and its interaction with the environment. After all, it is the interaction of a whole cloud ensemble with the large-scale flow that one needs to understand and to parameterize for large-scale weather and climate model purposes. Since there are only a few

observational field experiments dealing with this more global issue, one is more and more relying on numerical cloud resolving models, such as large-eddy simulation (LES) models, for this task. Therefore we will discuss the state of the art of LES modeling for shallow cumulus convection in section 5. Finally in section 6 we will see how all this knowledge has accumulated in parameterizations of cumulus convection for large-scale models.

2. Essentials of Thermodynamics of Cloudy Air

2.1. INTRODUCTION

Everyone who reads a book on atmospheric thermodynamics runs the risk of getting overwhelmed by a seemingly endless list of temperatures. However, in cloud physics, one essentially needs only three temperatures: one for dry adiabatic processes, one for moist adiabatic processes and one for measuring buoyancy. The purpose of this section is to give a simple self-contained introduction into the thermodynamics of cloudy air. For a more complete overview the reader should consult the standard work of Iribarne and Godson [22] or chapter 4 of Emanuel's book on Atmospheric Convection [14] which is more up to date. The content of this chapter is neither rigorous nor complete. Its sole purpose is to offer the reader not familiar with this field, necessary operational knowledge required for understanding the rest of this paper.

2.2. BASIC THERMODYNAMICS OF CLOUDY AIR

We consider an isothermal parcel with volume V, temperature T and a total mass m. It contains a mass m_d of dry air, m_v of water vapor and m_l of liquid water. Since the masses are additive, we can write the total density ρ as the sum of the partial densities

$$\rho = \frac{m}{V} = \rho_d + \rho_v + \rho_l. \tag{1}$$

In order to take the effect of water vapor and liquid water into account for the equation of state we use the gas law for dry air and water vapor

$$p_d = \rho_d R_d T \quad , \quad p_v = \rho_v R_v T, \tag{2}$$

where R_d and R_v are the specific gas constants for dry air and water vapor. If we apply Dalton's law (additivity of partial pressures), assuming that the liquid water does not have an effect on the pressure, we can write the total pressure as

$$p = p_d + p_v, \tag{3}$$

and consequently, the equation of state of a moist parcel, containing dry air, water vapor and liquid water as

$$p = \rho R_d T \left[1 + (\varepsilon^{-1} - 1)\frac{\rho_v}{\rho} - \frac{\rho_l}{\rho}\right], \tag{4}$$

where $\varepsilon = R_d/R_v \cong 0.622$. This result motivates the use of the specific humidity for water vapor q_v and liquid water content q_ℓ defined as

$$q_v \equiv \frac{\rho_v}{\rho} \quad , \quad q_\ell \equiv \frac{\rho_l}{\rho}. \tag{5}$$

We can rewrite the equation of state (4) in a similar form as (2) if we define a virtual temperature T_v

$$p = \rho R_d T_v \quad , \quad T_v \equiv T\left[1 + 0.61 q_v - q_l\right]. \tag{6}$$

Note that T_v can be interpreted as the temperature that dry air must have in order to have the same density as the moist air under consideration. Since for a given pressure, T_v is inversely proportional to the density, it is a direct measure of the buoyancy of an air parcel.

Inspection of (6) shows immediately that moist air ($q_v > 0$) has a higher virtual temperature than dry air ($q_v = 0$) at the same pressure and temperature and hence a lower density. Presence of moisture therefore enhances the buoyancy of a parcel. Liquid water however works in the opposite direction; it increases the density of an air parcel. Since typically $q_v \sim O(10^{-2})$ and $q_\ell \sim O(10^{-3})$, the effect of humidity on T_v is less than 1%. Nevertheless, in cloud dynamics (see subsection 5.4) it turns out that the buoyancy of a cloud, *i.e.* the virtual temperature excess, is largely determined by these subtle humidity effects.

Water vapor condensates into liquid water if it exceeds the saturation specific humidity q_s, which is the maximum amount of water vapor an air parcel can contain before condensation takes place. It can be written using (2) and (3) in terms of the total pressure and the saturation vapor pressure $e_s \equiv \rho_s R_v T$

$$q_s \equiv \frac{\rho_s}{\rho} = \varepsilon \frac{e_s}{p + e_s(\varepsilon - 1)}. \tag{7}$$

The saturation curve e_s can be found by integrating the Clausius-Clapeyron relation [22]

$$\frac{d \ln e_s}{dT} = \frac{L}{R_v T^2}, \tag{8}$$

where L denotes the specific latent heat of vaporization. As a first approximation L may be considered constant with temperature and equal to its

triple point value L_0. Integration of (8) from the triple point (e_0, T_0) then readily gives

$$e_s = e_0 \exp\left[-\frac{L_0}{R_v}(\frac{1}{T} - \frac{1}{T_0})\right], \tag{9}$$

with $e_0 = 6.107$ hPa, $T_0 = 273.15$ K, and $L_0 = 2.5 \times 10^6$ J/kg. More accurate solutions for the saturation curve can be found in [22, 14, 62]. The important observation to be made here is that the saturation specific humidity q_s, as defined by (7) is a function of p and T only, and is therefore a state variable.

2.3. CONSERVED VARIABLES

If one wants to study turbulent mixing of heat and moisture it is convenient to eliminate all internal sources and sinks. This can be done by absorbing these sinks and sources into the heat and moisture variables. Working with such "conserved" variables has the advantage that a mixture of two parcels can be easily desribed in terms of a linear combination of the properties of the two individual parcels. We will make explicitly use of this property in section 3.

In the absence of precipitation and the ice phase, condensational effects are the only sinks and sources of the humidity variables q_v and q_l. It is then easy to realise that the sum of these variables, the total water specific humidity

$$q_t = q_v + q_\ell, \tag{10}$$

is a conserved moisture variable, invariant for condensational processes and pressure changes.

For heat there are two sources and sinks that we want to eliminate by including them into a variable: 1) temperature changes due to adiabatic compression and expansion and 2) temperature changes due to condensational effects. We will introduce two temperatures: one that is conserved under "dry" adiabatic processes and another one that is also conserved under "moist" adiabatic processes, *i.e.* adiabatic processes including condensation. Combining the first and second principle of thermodynamics and again neglecting the ice phase and transitions of liquid water to precipitation, one can find for the specific entropy s of a parcel [14, 22, 62]

$$ds(p, T, q_\ell) = c_{pm} d\ln T - R_m d\ln p - \frac{L}{T} dq_\ell, \tag{11}$$

where $c_{pm} = c_{pd} + q_v c_{pv} + q_\ell c_{p\ell}$, and $R_m = R_d + q_v R_v$ are the mean parcel values for respectively the specific heat capacity and the specific gas constant (see Appendix B for precise values of the used constants). Note that

the last term of (11) represents condensational effects. No approximations are involved in the derivation of (11). However, for the purpose of shallow cumulus convection it is sufficient to work with an approximate form. We use the dry air values for the specific heat and the specific gas constant (*i.e.* $c_{pm} \sim c_{pd}$ and $R_m \sim R_d$) in (11) and furthermore approximate the last term in (11) by $d(L_0 q_\ell / T)$. For a discussion on the errors made using the above mentioned approximations we refer to Tripoli and Cotton [62].

In the absence of liquid water ($q_\ell = 0$) the last term in (11) vanishes and the remaining terms define the potential temperature θ as $ds \equiv c_{pd} d \ln \theta$. Integrating (11) from a reference state, usually defined by a reference pressure $p_0 = 1000$hPa gives

$$\theta = T \left(\frac{p_0}{p} \right)^{\kappa} \equiv T \pi^{-1}, \tag{12}$$

where $\kappa = R_d / c_{pd}$ and π is the Exner function. The potential temperature θ can be interpreted as the temperature an air parcel would obtain if compressed or expanded adiabatically to a pressure of 1000 hPa. It is therefore conserved during adiabatic processes ($ds = 0$) without phase changes ($dq_\ell = 0$). We will refer to such processes as dry adiabatic processes.

If we include phase changes, we can define the potential liquid water temperature θ_l by $ds = c_{pd} d \ln \theta_l$ [6]. Integration of the approximate form of (11) from a reference state defined by $p_0 = 1000$hPa and $q_l = 0$ gives

$$\theta_\ell = \theta \, \exp \left(- \frac{L_0 q_\ell}{c_{pd} T} \right). \tag{13}$$

Within the approximations mentioned, θ_l is conserved under moist adiabatic processes ($ds = 0$), including phase changes.

The liquid water potential temperature θ_ℓ has advantages above the still widely used equivalent potential temperature θ_e. Firstly, θ_ℓ is especially useful as a model variable since it reduces to the (dry) potential temperature in the absence of liquid water. Secondly, since $q_\ell \sim O(10^{-3})$ in clouds, the term in the exponent of (13) is always much smaller than 1 so one can use a linearized version of θ_ℓ by employing a Taylor expansion

$$\theta_\ell \approx \theta - \frac{L_0}{c_{pd} \pi} q_\ell. \tag{14}$$

As an alternative for θ and θ_ℓ one can also use the so-called static energies, which in the next section will be proven to be useful for finding lapse rates. They are easily derived from (11), assuming hydrostatic equilibrium $dp = -\rho g dz$ and the gas law (6)

$$dh(T, z, q_\ell) = c_{pm} dT + g dz - L dq_\ell. \tag{15}$$

Although this can be integrated exactly [14], we will approximate the specific heat again by its dry air value ($c_{pm} \sim c_{pd}$) and L by its triple point value L_0. Integration gives for the unsaturated case (*i.e.* $dq_\ell = 0$) the *dry* static energy,

$$h_d = c_{pd}T + gz, \tag{16}$$

and for the saturated case the *liquid* water static energy

$$h_\ell = c_{pd}T + gz - L_0 q_\ell. \tag{17}$$

The static energies h_d and h_ℓ are closely related to θ and θ_ℓ. The dry static energy h_d is (as θ) conserved under unsaturated adiabatic transformations whereas the liquid water static energy h_l (as θ_ℓ) is also conserved under saturated adiabatic transformations. The only additional assumption that went into the derivation of the static energies is that the pressure change should be strictly hydrostatic.

2.4. LAPSE RATES

If a dry air parcel is lifted dry adiabatically it cools due to expansion. The rate at which the temperature is decreasing is given by the dry adiabatic lapse rate Γ_d. Since the dry static energy h_d is constant for such adiabatic vertical displacements, (16) immediately gives for the dry adiabatic lapse rate

$$\Gamma_d \equiv -\left(\frac{dT}{dz}\right)_{parcel} = -\left(\frac{\partial T}{\partial z}\right)_{h_d} = \frac{g}{c_{pd}} \cong 9.76\text{K/km}. \tag{18}$$

If a saturated parcel is lifted adiabatically it will condensate and, due to the resulting latent heat release, the temperature will not fall as rapidly as in the unsaturated (dry) case. To calculate this moist adiabatic lapse rate we substitute $q_\ell = q_t - q_{sat}(p,T)$ in (17). This way h_ℓ is only a function of z, p and T. Using hydrostatic equilibrium plus the fact that h_ℓ and q_t remain constant along a moist adiabat, we find for a saturated parcel, using (17), (7) and (9)

$$\Gamma_m \equiv -\left(\frac{dT}{dz}\right)_{parcel} = -\left(\frac{\partial T}{\partial z}\right)_{h_\ell, q_t} = \frac{g}{c_{pd}} \frac{\left(1 + \frac{Lq_s}{R_d T}\right)}{\left(1 + \frac{L}{c_p}\frac{\partial q_s}{\partial T}\right)} < \Gamma_d. \tag{19}$$

The moist adiabatic lapse rate Γ_m is always smaller than the dry adiabatic lapse rate Γ_d. Its actual value however depends strongly on temperature. For $T = 290$ K and $p = 1000$ hP we find $\Gamma_m = 4.5$ K/km, much smaller than Γ_d. For lower temperatures, however, the difference between Γ_m and Γ_d becomes progressively smaller.

2.5. LOCAL STABILITY OF THE ATMOSPHERE

The presence and intensity of convection is largely determined by the thermodynamic stability of the atmosphere. This stability is usually defined by the sign of the buoyancy of a vertically displaced atmospheric parcel. More precisely, given average profiles of $\overline{T}$ and $\overline{q_t}$, we consider a parcel at a height z_0 with the average atmospheric properties at that height and displace it vertically an infinitesimal distance δz. The resulting vertical velocity w is then given by Newton's second law of motion

$$\frac{dw}{dt} = \frac{d^2\delta z}{dt^2} = B\left(z + \delta z\right) \cong \frac{dB}{dz}\delta z, \tag{20}$$

where the buoyancy force per unit mass B working on the displaced parcel is given by

$$B = -g\frac{\rho_p - \overline{\rho}}{\rho_p} = g\frac{T_{v,p} - \overline{T_v}}{\overline{T_v}}, \tag{21}$$

where the subscript p denotes parcel properties. In the last step of (21) we used the equation of state (6) and assumed that the parcel's pressure adjusts instantaneously to the environmental pressure, *i.e.* $p_p = \overline{p}$. In (20) we recognize the equation of the harmonic oscillator whose solution is either oscillating or exponentially growing, depending on the sign of dB/dz. Therefore, it is natural to define the local stability of the atmosphere at a height z_0 as

$$\begin{aligned} \frac{d\overline{T}_v}{dz} > \frac{dT_{v,p}}{dz} &\Longleftrightarrow \text{stable} \quad , \\ \frac{d\overline{T}_v}{dz} < \frac{dT_{v,p}}{dz} &\Longleftrightarrow \text{unstable} \quad , \end{aligned} \tag{22}$$

which means that one has to compare the lapse rate of T_v of a parcel with the vertical gradient of the atmospheric profile of T_v. The virtual temperature lapse rate can be calculated along the same lines as the temperature lapse rates in the previous subsection. Ignoring for simplicity effects due to the vertical gradient of $\overline{q}_t$ it is easy to see that for an unsaturated atmosphere at z_0, the borderline between stable and unstable is simply given by the *dry* adiabatic lapse rate Γ_d, while for a saturated atmosphere it is the *moist* adiabatic lapse rate Γ_m.

This property allows the introduction of an important concept of conditional instability. Suppose that locally the atmosphere has a vertical temperature gradient in between a moist and dry adiabat such as schematically illustrated in Fig. 2. This implies that the atmosphere at such a point is

stable for unsaturated parcels but unstable for saturated parcels. In that case we speak of conditional instability which can be formulated as

$$\begin{aligned} (-\partial\overline{T}/\partial z) > \Gamma_d \quad &\Longleftrightarrow \quad \textit{Absolute instability} \\ \Gamma_m < (-\partial\overline{T}/\partial z) < \Gamma_d \quad &\Longleftrightarrow \quad \textit{Conditional instability} \\ (-\partial\overline{T}/\partial z) < \Gamma_m \quad &\Longleftrightarrow \quad \textit{Absolute stability.} \end{aligned} \tag{23}$$

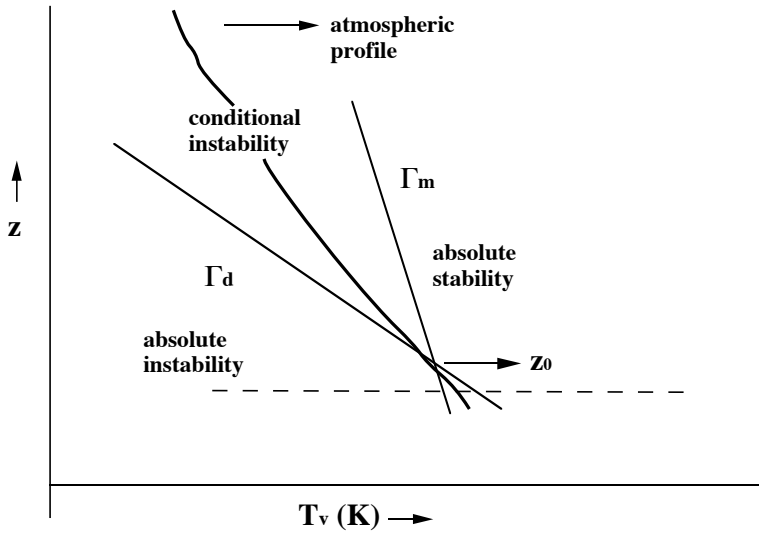

Figure 2. A conditional unstable profile together with a dry and a moist adiabat.

Although conditional instability is a purely mathematical concept, it is a typical property of the atmosphere in the cloud layer; while saturated cloud parcels are unstable with respect to vertical pertubations, unsaturated parcels are stable. The concept of local conditional instability should not be mistaken for conditional instability of atmospheric layers in which finite-amplitude displacements are considered. This is the topic of the next subsection.

2.6. THE PARCEL METHOD AS A POOR MAN'S CLOUD MODEL

We will now proceed to investigate finite-amplitude displacements of parcels and see that the concept of conditional instability has special consequences for moist convection. This is most easily illustrated by considering a typical vertical profile of the virtual potential temperature for a trade-wind-cumulus-topped boundary layer. Such a profile is schematically illustrated in Fig. 3. Near the surface there is a thin absolutely unstable layer, the

surface layer, above which lies a dry convective boundary layer. On top of this subcloud layer there is a conditionally unstable cloud layer in which cumulus clouds are formed. Finally, an absolutely stable inversion layer lies on top.

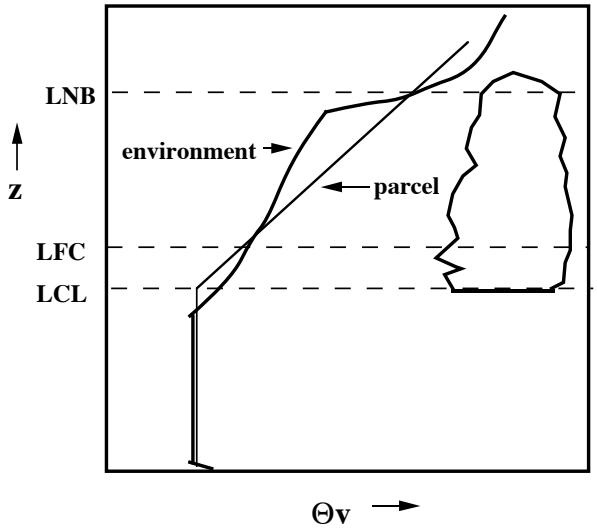

Figure 3. A schematic environmental profile of $\overline{\theta}_v$ for a cumulus topped boundary layer along with a θ_v profile for a parcel that is released from the surface layer.

As a metaphore for a rising thermal, we release a parcel from the surface layer with thermodynamic properties $\overline{T}_0$ and $\overline{q}_{t,0}$ of that layer. As the parcel rises it will cool with a lapse rate of 9.8 K/km until it gets oversaturated at the *lifting condensation level* (LCL). Note that at this point the parcel is negatively buoyant, and would simply fall back unless it has enough kinetic energy to continue. If that is the case it will continue rising but with a moist adiabatic lapse rate as given by (19), since it has a "condensation engine" aboard. Because the cloud layer is conditionally unstable, the moist adiabat describing the parcel's temperature must intersect the atmospheric profile. This occurs at the so-called *level of free convection* (LFC) where the parcel becomes positively buoyant with respect to the environment. From this point on the parcel can rise freely until the moist adiabat crosses the profile again in the inversion layer at the *level of neutral buoyancy* (LNB). Possibly, due to accumulated kinetic energy, the parcel can penetrate slightly further into the inversion (overshoot). Viewing a parcel as a rising thermal, it can serve as a poor man's cloud model and the LCL and the LNB can be used as estimates for cloud base and cloud top, respectively.

This example shows that for finite-displacements the stability of a parcel depends on the origin z_0 of the parcel. Therefore, as a sort of non-local

integrated stability function, one can define the *convective available potential energy* (CAPE) as the buoyancy of a parcel, integrated from the height z_0 where it is released to its to its actual position

$$CAPE\,(z, z_0) \equiv \int_{z_0}^{z} B dz = R_d \int_{p(z)}^{p(z_0)} (T_{v,p} - \overline{T}_v) d\ln p, \qquad (24)$$

which is directly related to the area between the two curves drawn in Fig. 3. CAPE can be considered as a measure of how much energy there is potentially available for moist convection, but it does not provide a clue on the actual release of this potential energy.

One may wonder why there is positive CAPE in the cloud layer anyhow. This is due to the fact that the region between the LCL and the LFC acts as a potential energy barrier for a parcel lifted from near the surface. This prevents a parcel to rise from the dry boundary layer into the cloud layer, *unless* it has enough kinetic energy to overcome this barrier. So due to this potential barrier, positive CAPE accumulates in the cloud layer as it is not directly consumed and transformed into kinetic energy by cumulus clouds. This leaves us with the physical picture of instabilities diagnosed by CAPE being build up slowly by radiative cooling and surface heating. The CAPE is occasionally consumed if a strong thermal overcomes the barrier and activates a cloud. In that case, the potential energy is transformed into kinetic energy by the cloud dynamics.

The mechanism that activates cumulus convection is called the trigger function [27] and is still a matter of debate, especially for the case of deep convection. In the case of shallow convection where CAPE in general is not so large, *i.e.* the potential barrier is quite small, the trigger is a local phenomenon caused by small perturbations such as local thermals that are strong enough to overcome the barrier.

It is the presence of the potential barrier that makes cumulus convection so much more intermittent in space and time than turbulence in the dry convective boundary layer; cloud updrafts occur in bursts in an otherwise quiet cloud layer. Another consequence is that the dynamics of vertical motions is quite different. Strong saturated updrafts in narrow unstable cloud channels and relatively weak unsaturated downdrafts in the stable environment give a highly positively skewed vertical velocity distribution which should be contrasted with the more classical Kolmogorov turbulence in the dry boundary layer. Figure 4 sums up these differences in a cartoonlike fashion.

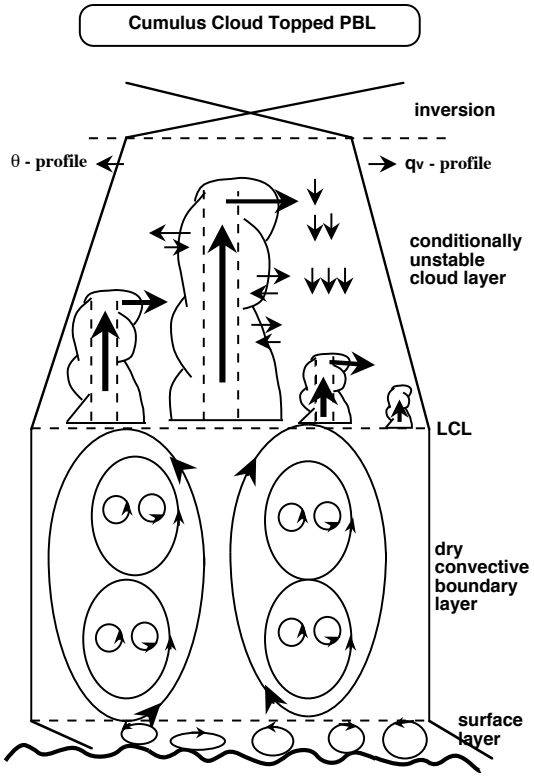

Figure 4. Cartoonlike view of the dynamics of the cumulus topped boundary layer.

3. Mixing and Dynamics of Individual Clouds

3.1. INTRODUCTION

If one observes a cumulus cloud, it is easy to recognize various stages of its life cycle such as sketched schematically in Fig. 5. First, a cloud may be born due to a strong rising thermal in the convective boundary layer that reaches the LCL. If during this first stage, the ascending cloud top is between the LCL and LFC we speak of a *forced cloud* [56] because it is still negatively buoyant and mechanically forced by subcloud thermals below. If the kinetic energy is large enough, the cloud will overcome the potential barrier and reach the LFC after which it becomes positively buoyant. The cloud is then in its *active phase* where rapidly growing turrets with sharp interfaces are visible. This development continues until the cloud attains its mature stage when it reaches its maximum height around or slightly above its neutral buoyancy level (LNB). If finally the fueling of moist air from the subcloud layer below ceases (possibly due to downdrafts induced by the cloud itself), the cloud enters its *passive stage*. During this decaying

phase the original cloud base disappears, the cloud interface becomes fuzzy and the cloud will dissolve by evaporation.

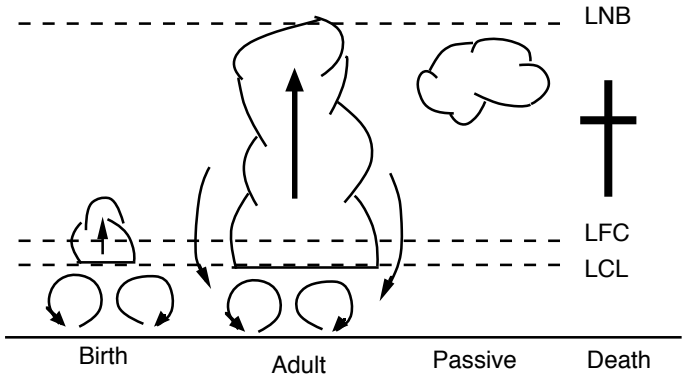

Figure 5. Schematic life cycle of a cumulus cloud.

A cloud could simply be described as a rising parcel if, during its active phase, it behaved simply as a burst of subcloud air that is injected into the conditionally unstable layer *without* mixing with its environment and finally detraining by evaporation at the LNB. In that case, modeling of vertical transport of moisture and heat would be straightforward, using the parcel concept introduced in section 2.6.

However, in reality matters are more complicated. Since the work of Stommel [55] it is known that clouds continuously mix air with their environment. More specifically, it was shown by Warner [65] that the liquid water content q_l, measured during many penetrations of cumulus clouds at various heights, is substantially lower than its adiabatic value based on the parcel method. Moreover, it was found that the ratio of the measured liquid water to its adiabatic value decreases systematically with height. This classic result has been confirmed by other authors, at least qualitatively [40, 25], and is an indication that clouds continuously dilute by turbulent mixing with their environment. This process which is usually referred to as *entrainment* and which will be made mathematically precise in section 6, directly affects cloud top height, vertical velocity and in-cloud fields. It is therefore crucial to understand the dynamics and mixing mechanisms of cumulus clouds with their environment. This will be the main theme of the remainder of this section. A review on entrainment in cumulus clouds from a more experimental point of view has been given recently by Blyth [8].

3.2. LATERAL MIXING

The first cloud models, developed in the sixties [54, 47, 48, 49], were all based on models of plumes and thermals [63]. The essence of all these models is that the picture of a rising parcel is extended to include *lateral* mixing of the parcel with its environment during the ascent.

Rather than giving the classic plume similarity arguments to calculate the effects of lateral entrainment, we proceed here by giving some simple hand-waving arguments. In this way we avoid the discussion to what extent plume models can be used for cloud modeling. Consider a cloud with upward rising air with a velocity w_c, which is entraining air laterally from the environment (see Fig. 6a). Further we make the assumption that the entrained environmental air homogenizes instantaneously with the cloudy air. As a result we can use the so-called "top-hat" approximation for thermodynamic variables $\phi = \{\theta_\ell, q_t\}$. This implies that at a height z, ϕ can take only two values, ϕ_c in the cloud and ϕ_e in the environment. Since the only way a conserved variable ϕ_c can change is through lateral mixing, we can write the Lagrangian time derivative of a rising parcel in the general form

$$\frac{d\phi_c}{dt} = F_{mixing}, \tag{25}$$

where we are searching an expression for F_{mixing}. The only parameters available are ϕ_c, ϕ_e and a time scale τ. Since we have no additional knowledge, we choose the simplest form for F_{mixing} and assume that the cloud dissolves by lateral mixing in a typical cloud life-time τ

$$F_{mixing} = -\frac{\phi_c(z) - \phi_e(z)}{\tau}. \tag{26}$$

If furthermore we assume steady-state and substitute (26), we can write (25) in the more familiar form

$$\frac{\partial \phi_c}{\partial z} = -\frac{1}{w_c \tau}(\phi_c - \phi_e) \equiv -\varepsilon(\phi_c - \phi_e), \tag{27}$$

where ε is usually referred to as the fractional entrainment rate. A more fundamental derivation of (27) is given in section 6.4. The result (27) allows a simple physical interpretation for ε. Realizing that a shallow cumulus cloud typically makes one eddy turnover, we can interpret the cloud life-time τ as the eddy turnover time. In that case, ε^{-1} is proportional to the vertical size h_c of the cloud

$$\varepsilon = \frac{1}{w_c \tau} \sim \frac{1}{h_c}. \tag{28}$$

We can use (28) to make an order of magnitude estimate for ε. If we take $\tau = 10^3$s and $w_c = 1\text{ms}^{-1}$ we find

$$\varepsilon \sim 10^{-3}\text{m}^{-1}. \tag{29}$$

Similarity arguments for plumes give the same result (27), but additionally with a quantitative estimate for the fractional entrainment rate [63]

$$\varepsilon = \frac{2\alpha}{R}, \tag{30}$$

where R is the radius of the plume and α is a dimensionless constant close to 0.1, a value determined from plumes in laboratory experiments. The use of this result in cloud models is, though still being common practice, highly questionable [43].

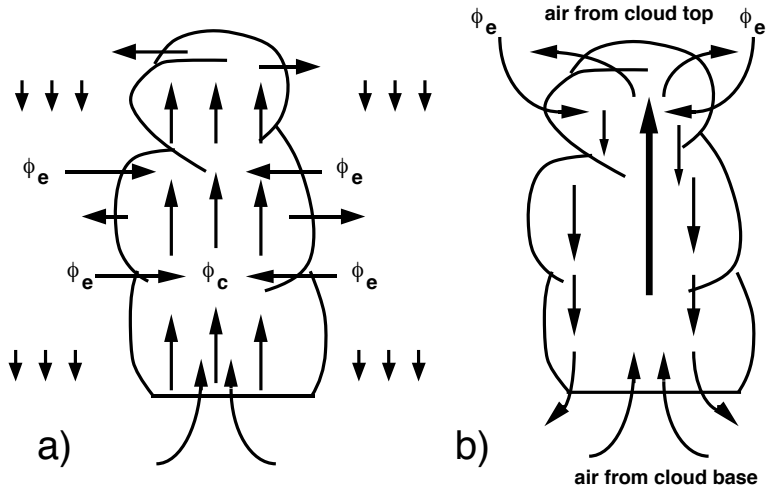

Figure 6. Schematic sketch of two extreme mixing mechanisms: a) *lateral mixing* where environmental air is continuously entrained into upward rising cloud air and b) *vertical mixing* where environmental air mixes with cloud air only near cloud base and cloud top.

3.3. VERTICAL MIXING

The concept of lateral entrainment has received considerable criticism over the last 25 years. A fundamental problem was pointed out by Warner [66]. Comparison of a lateral entraining cloud model with cloud measurements showed that (27) can not simultaneously produce a realistic liquid water content and a cloud top height. Adjusting increasing ε in order to get a

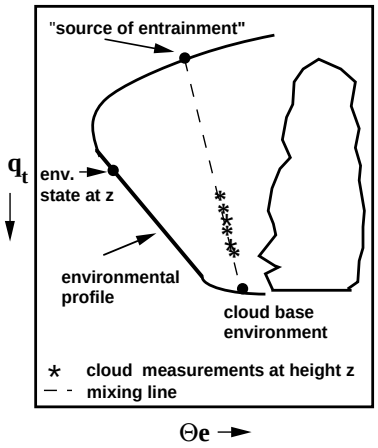

Figure 7. Schematic conserved variable diagram with a environmental sounding and in-cloud data points (∗) measured at height z that fall on a straight mixing line. The upper intersection point of the mixing line with the sounding is usually interpreted as the source of entrainment.

realistic liquid water content predicted a too low cloud top height (*i.e.* LNB). Vice versa, reduction of ε gave a correct cloud top but a too high liquid water content. A second riddle was the observation of strong random fluctuations of liquid water in the cloud with no systematic variations from cloud edges towards the middle, which is hard to explain with a simple lateral entraining cloud model.

This gave rise to the idea, already suggested by Squires [53], that vertical rather than lateral mixing is the principal mechanism for diluting cumulus clouds. In this view a cloud consists of relatively undiluted updrafts that entrain environmental air only at cloud base and at the zero buoyancy level near the maximum cloud top. Subsequently, evaporation will induce negatively buoyant *penetrative downdrafts* in the cloud through cloud top instability (Fig. 6b).

Empirical thermodynamical evidence for such a vertical mixing mechanism was presented by Paluch [38]. The idea is presented in Fig. 7 which shows an idealized conserved variable diagram of a typical environmental sounding in terms of the conserved variables q_t and the equivalent potential temperature θ_e (which could have been θ_l equally well), defined by

$$\theta_e = \theta \, \exp\left(\frac{L_0 q_v}{c_{pd} T}\right) . \tag{31}$$

Comparing (31) with the definition of θ_ℓ (13) shows that these two temperatures differ only by q_t in the exponent. Therefore, if θ_ℓ and q_t are conserved

variables, so is θ_e.

A conserved variable diagram has the advantage that mixing of two different parcels results in a mixed parcel which falls on a *mixing line*, *i.e.* a straight line connecting the thermodynamic states of the two original parcels. The position of the final mixture on this mixing line is determined by the relative concentrations of the original parcels. Therefore, if cloud air would consists of a two-point mixture of cloud base air and cloud top air, as suggested by Squires [53], in-cloud measurements at a specific height would scatter on a straight mixing line which connects the environmental sounding at cloud base and cloud top (Fig. 7).

By applying this analysis to sailplane measurements inside developing cumuli congestus in Colorado, it was found indeed that cloud data scattered fairly well on a straight line between cloud base and a point (the so-called source of entrainment) several kilometers above the level of observation [38]. These results were interpreted as empirical evidence for vertical mixing of undiluted air from cloud base with environmental air near cloud top through penetrative downdrafts. This view, in some sense the opposite extreme from the lateral entraining plume, resolved the paradox raised by Warner [66] and also explained qualitatively the strong fluctuations of the liquid water which could be induced due to evaporation in the penetrative downdrafts.

3.4. ASCENDING CLOUD TOP ENTRAINMENT

The rather extreme picture of vertical mixing is nevertheless not without problems. Conceptually it is rather odd since it suggests that clouds would only entrain once they have reached their maximum cloud top. Since Paluch [38], numerous studies have been reported that used the same analysis to infer the source of entrainment, with rather ambiguous conclusions. Some studies claimed that the source of entrained air originated near the cloud top [29, 4, 23, 39], but also entrainment sources were reported near the observation level [41, 9, 7]. In most cases the source level was less than 1 km from the level of observation.

A more refined view was put forward by Blyth *et al.* [7] as a result of a study of more than 80 continental cumulus clouds above Montana. A compilation of 44 cases is shown in Fig. 8 and shows that the source of entrained air was only slightly above ($\sim$500 m) the level of observation. No dependence of the source level on the existence of up- and downdrafts was found. These findings favor a picture of a shedding thermal for cumulus convection such as sketched in Fig. 8. The top of the cloud consists of a undiluted rising core with a toroidal circulation. This advancing cloud top is inducing mechanically forced downdrafts of the environmental air that is mixed with the core slightly below the advancing top. The resulting mixed

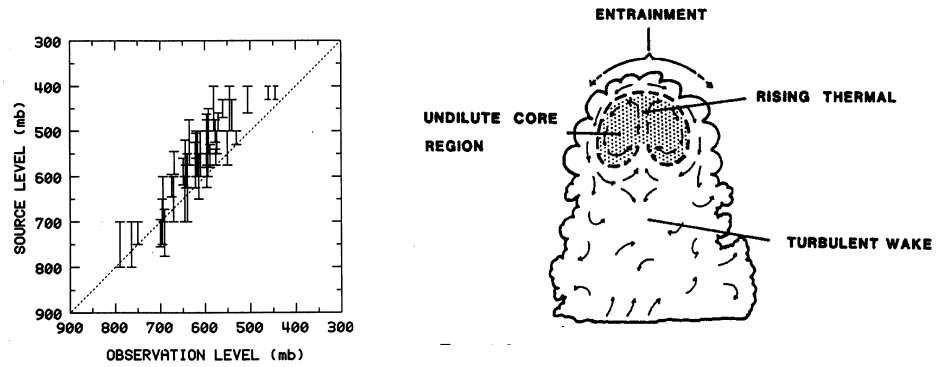

Figure 8. Left panel: A scatter plot of the height of the "source of entrainment" vs. the height of the observation level for 44 different cases using the "mixing line" analysis as explained in Fig. 7. Right panel: Interpretation of the scatter plot leading to a schematic view of a cloud as a shedding thermal. See text for further discussion [7].

parcels have a reduced buoyancy and are left behind in a trailing wake *and stay there.* With this mechanism the mixed air at each level consists of two-point mixture of cloud base air (the undiluted core) and environmental air slightly above the level of observation, in agreement with the observed mixing line.

The weak point of the proposed mechanism is that only undiluted cloud air from the cloud base mixes with the environmental air. Indeed it is true that undiluted air has been found at all levels within cumulus clouds [17, 23] but this air represents only a small fraction of the cloud. It is then difficult to understand how only this small undiluted core region participates in all mixing events with the environment.

3.5. PALUCH ANALYSIS REINTERPRETED; BACK TO AN ENTRAINING PLUME MODEL?

Although the interpretation of straight lines as two-point mixing is tempting due to its simplicity, one should be extremely cautious with it. As pointed out by Taylor and Baker [58] a rather linear distribution of in-cloud (θ_e, q_t) data points can equally well be interpreted as a result of any buoyancy sorting mechanism. Their point is illustrated by drawing a zero buoyancy line in a conserved variable diagram. Such a line consists of all possible combinations of θ_e and q_t that have the same θ_v as the environment at the level of observation. The point is that this zero buoyancy line lies quite close to a mixing line between cloud base and the level of observation. In fact, in-cloud measurents are not decisive enough to discriminate statistically between these two lines. Therefore an alternative interpretation of

the straight mixing lines is simply that most cloud parcels are close to their zero buoyancy level. This picture favors the buoyancy sorting mechanism which assumes that all parcel mixtures are en route to their zero buoyancy level. Apparently, parcels with considerable buoyancy excess are so unstable that they are quickly transported to their zero buoyancy level and consequently are quite rarely observed.

Additional evidence for this latter interpretation has been given recently by Lin and Arakawa [30] who performed a Paluch analysis on the output of a 2-D cloud-resolving model. When the data points in a cloud are plotted in a conserved variable diagram they are distributed on a quasi-straight line that intersects the sounding close to the level of observation. Naively one might interpret this as a two-point mixing of cloud base air with environmental air near the observation level. However, by calculating the backward trajectories it was shown that the cloud air originated from *multiple* levels, all *below* the level of observation.

These results put both the extreme vertical mixing mechanism and the shedding thermal model of Blyth [7] in jeopardy since both views lean heavily on the two-point mixing interpretation. Since observational thermodynamic evidence is apparently not sufficient we discuss next some direct kinematic cloud observations.

Aircraft observations of trade wind cumulus bands off the coast of Hawaii were analyzed by Raga *et al.* [40]. For active clouds below the inversion they found that vertical velocities were almost exclusively positive. Only above the inversion equally strong downdrafts were observed. Similar results were found by Jonas [25] who studied small maritime cumulus clouds over the North sea. Traverses through active cumuli showed organized updrafts in the clouds with only a thin shell of downdrafts of around 2 m/s outside the clouds. The values of θ_ℓ and q_t in the downdrafts were not too different from the far field values at the observation heights. This led to the conclusion that the descent around the cloud edges is due to mechanical forcing rather than penetrative downdrafts driven by evaporative cooling. These results are supported by numerical simulations of Klaassen and Clark [28].

In view of these findings the following picture emerges. Following Blyth *et al.* [7], an active cumulus cloud can still be viewed as a rising thermal with a *lateral entraining ascending cloud top*. However, we can relax the condition that only undiluted air rises and mixes with the environment and that mixed air stays behind in a trailing wake. Instead, the rising thermal exists of different mixtures, ranging from the most buoyant undiluted parcels to nearly zero buoyant mixtures. Only when a mixture becomes negatively buoyant it will stay behind and eventually detrain by evaporation. This is essentially the same mechanism as proposed by Taylor and Baker [58].

It does not suffer from the Warner paradox [66] since the cloud top is determined by the undiluted parcels while other parcels dilute the cloud by lateral entrainment. It gives quasi-linear mixing lines [58] and is qualitatively in agreement with the observed kinematics. Ironically enough, this picture of what we will call an *intermittent entraining thermal* is not that different from the old classic plume models. The main difference is that in the present picture the lateral entrained air is assumed *not* to homogenize with the rest of the cloud air instantaneously.

3.6. MODELS FOR MIXING IN CUMULI

Since there is still no consensus on what is the principal mechanism of entrainment (and detrainment) in cumulus clouds, there coexist a wide range of models and schemes, each emphasising different aspects of the mixing mechanism. In order to categorize the various schemes in a comprehensible way it is convenient to introduce two time scales:

- τ_h as the typical time to homogenize lateral entrained air with cloud air, and
- τ_c as cloud life time, *i.e.* $\tau_c \sim h_c/w_c$ where h_c is the vertical size of the cloud and w_c the typical vertical velocity in the cloud (see (28)).

In the extreme case that $\tau_h \ll \tau_c$, lateral entrained air is immediately homogenized with cloudy air at that height. Then, it is sufficient to work only with cloud averaged values. This is the basic assumption of the classic entraining plume model introduced in section 3.2. On the other side of the spectrum we have the situation that $\tau_h \gg \tau_c$. This implies that the entrained air is mixing so slowly with the cloudy air, that it can only take place near the zero buoyancy level where the vertical velocity goes to zero. Therefore this limit covers the vertical mixing case, as described in section 3.3 where cloud air essentially mixes with environmental air only at the maximum cloud top after which the mixture sinks back to its zero buoyancy level. This idea has been translated into a simple model first by Telford [59].

Most models and schemes that have been proposed over the last 10 years are in between these two extremes. If $\tau_h \sim \tau_c$, entrained air can travel a considerable distance in the vertical before being homogenized with the rest of the cloud. Therefore it is necessary to use a probability density function of the cloud fields, or equivalently, an ensemble of rising and descending cloud parcels. We will refer to these class of models as *stochastic* [42] or *episodic* [13]. The essence of all these models is that the cloud is represented by an ensemble of parcels, each one having a different mixing fraction with environmental air (see Fig. 9). Each parcel is then sent to its zero buoyancy level whereafter it is assumed to detrain by evaporation. Since there is a

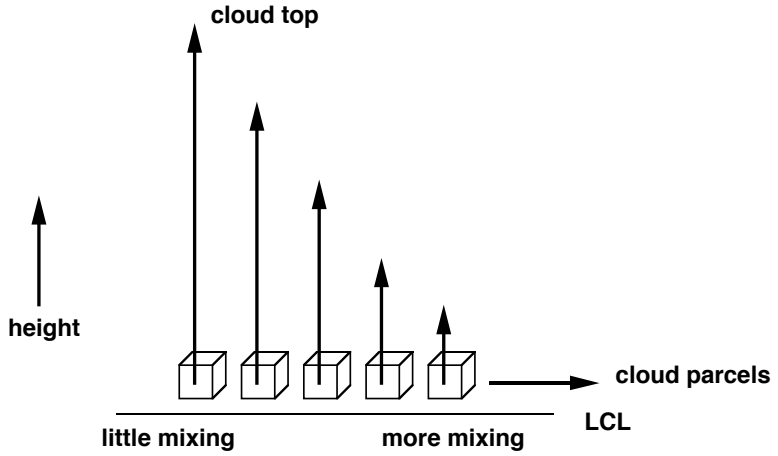

Figure 9. Principle of stochastic mixing. The cloud is modeled as a ensemble of mixtures, each one having different mixing fractions with environmental air. See text for further discussion.

lot of free parameters in this approach, many variations on this theme are possible and indeed have been formulated [13, 42, 26, 21].

A model that despite its simplicity captures some essential features of the intermittent entraining thermal described in section 3.5 is the cloud model proposed by Kain and Fritsch [26]. It essentially consists of a rising plume model where at each level equal amounts of cloudy and environmental air are used to make an ensemble of mixtures that is assumed to be Gaussian distributed. The negatively buoyant mixtures are assumed to detrain while the positive buoyant mixtures are mixed into the plume updraft.

4. Observational Large-Scale Budgets of Cloud Ensembles

Present state of the art global circulation models (GCM) have a typical resolution of 100 km. For shallow cumulus convection this implies that a suitable parameterization should take into account the statistical effect of a whole cloud ensemble rather than the dynamics of individual clouds. On the one hand, this is a complicating factor since various clouds may differ substantially, most importantly, in size. Dependent on the initial conditions at cloud base, clouds can reach quite different maximum heights. On the other hand, it facilitates parameterizations since one does not have to consider individual cloud life cycles.

Ideally, to study the effect of a cloud ensemble on the large-scale flow, one ought to analyze large-scale budgets based on observations. Unfortunately, only a few large-scale budget studies are reported. Notable examples

are studies based on the undisturbed periods of field experiments such as BOMEX [18, 19, 36, 15], ATEX [3] and more recently TOGA COARE [24].

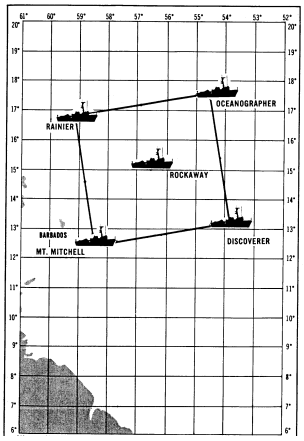

Figure 10. Map of the fixed ship array during BOMEX.

The usual strategy to derive large-scale budgets form such field experiments is still by means of rawinsonde data. As an example, consider the undisturbed period of the Barbados Oceanographic and Meteorological Experiment (BOMEX). Figure 10 shows the fixed ship locations from which soundings were taken each 1.5 hour during BOMEX. The large-scale vertical velocity, *i.e.* the subsidence, can be obtained from the area averaged continuity equation, which, after employing the divergence theorem, is

$$\oint \hat{\mathbf{n}} \cdot \mathbf{v} dl + \frac{\partial \overline{w}}{\partial z} = 0, \tag{32}$$

where $\mathbf{v}$ denotes the horizontal velocity vector, w the vertical velocity and bars indicate area averages. The contour integral is taken along the fixed ship array and $\hat{\mathbf{n}}$ denotes an outward pointing normal unit vector along the contour. Just for the sake of simplicity we assume a constant density. Since the contour integral can be estimated using the rawinsonde data, the large-scale subsidence $\overline{w}$ can be obtained as a residual.

The area averaged budget equations for heat and moisture are

$$\begin{aligned} \frac{\partial \overline{\theta}}{\partial t} + \overline{\mathbf{v}} \cdot \nabla \overline{\theta} + \overline{w} \frac{\partial \overline{\theta}}{\partial z} &= -\frac{\partial \overline{w'\theta'}}{\partial z} + \frac{\pi L}{c_p}(c - e) + Q_R \equiv Q_1, \\ \frac{\partial \overline{q_v}}{\partial t} + \overline{\mathbf{v}} \cdot \nabla \overline{q_v} + \overline{w} \frac{\partial \overline{q_v}}{\partial z} &= -\frac{\partial \overline{w'q_v'}}{\partial z} - (c - e) \equiv -Q_2, \end{aligned} \tag{33}$$

where primes denote deviations from the area averages, and Q_R is the heating rate due to radiation. All the terms on the left hand side of (33) can be obtained by rawinsonde data: the storage term (first term), the large-scale advection term (second term) by employing the divergence theorem and, most importantly, the subsidence term (third term) by using the already diagnosed subsidence $\overline{w}$. As a result, the so-called subgrid processes on the right hand side of (33) are obtained as an overall residual. Historically, these residuals are referred to as the apparent heat source Q_1 and the apparent moisture sink Q_2. They consist of a turbulent flux divergence term (first term) that describes the vertical transport of heat and moisture, a net condensation term $c - e$ (second term) and, in case of the heat equation, an additional radiative heating term Q_R.

Usually during field experiments such as BOMEX, measured surface fluxes of heat and moisture are also available. These can be related to Q_1 and Q_2 by a vertical integration of (33)

$$\begin{aligned} \int_0^\infty (Q_1 - Q_R)dz &= (\overline{w'\theta'})_{srf}, \\ \int_0^\infty Q_2 dz &= -(\overline{w'q_v'})_{srf}, \end{aligned} \tag{34}$$

and provide an additional integral check for the diagnosed subgrid processes.

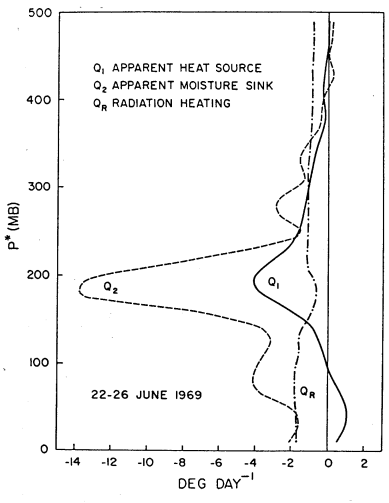

Figure 11. Observed Q_1, Q_2 and Q_r for the undisturbed BOMEX period (from Nitta and Esbensen [36]).

The above described analysis method is not without problems. The left hand side of (33) is in general dominated by the subsidence term, even for the case of a typical divergence of only 5×10^{-6} s^{-1} (corresponding to a subsidence of only 5×10^{-3} ms^{-1} at 1000 m). Such a small divergence can only be diagnosed by (32) if there is a persistent subsidence. This was the case during the undisturbed period of BOMEX where a 4-day stationary state was observed. A summary of the large-scale budget analysis is shown in Fig. 11. Due to subsidence a strong large-scale drying and heating was diagnosed. Since the storage term was small it can be concluded that this large-scale forcing was counteracted by a mixture of turbulent transport, condensational processes and radiative cooling such as diagnosed by Q_1 and Q_2.

In conclusion, observations give at best an estimate for the *overall* subgrid processes such as expressed by Q_1 and Q_2. This is useful information for evaluating models and parameterizations but certainly not enough for a fundamental understanding of the physical processes that are at play and which are needed to design a parameterization on a physically sound basis. Ideally, one would like to have information on how the subgrid processes are build in terms of turbulent fluxes and condensational heating. For this purpose we have to resort to numerical cloud resolving models such as large-eddy simulation (LES) models. This is the topic of the next section.

5. LES Modeling of Shallow Cumulus Convection

5.1. INTRODUCTION

The resolution of a large-eddy simulation (LES) model is such that the largest eddies of a three-dimensional turbulent field are explicitly resolved. Therefore, the bulk of the turbulent field is resolved by the model and the dynamics of the smaller subgrid eddies can be expressed realistically in terms of the resolved eddies, due to the well-known scaling behavior in the inertial subrange. This approach, pioneered by Deardorff [12], has been successfully applied to the dry convective boundary layer for which it was originally designed (see paper of Nieuwstadt [35] in this volume). Sommeria [51] was the first one to use an LES model to study a cumulus-topped boundary layer by including a condensation scheme. Various LES studies of shallow cumulus cases have been reported since then [52, 5, 10, 33, 11, 43]. In this section we will mainly discuss LES results based on BOMEX such as reported in [43] for the following reasons:

- BOMEX describes a shallow cumulus case that is *typical* for the whole trade-wind region, which makes it more universal than "just a case".
- During the undisturbed phase of BOMEX a well-defined steady state of the atmosphere was observed and realistic estimates of the large scale

forcing could be made. This provides a *critical* test for an LES model, since it has to produce a realistic cumulus cloud dynamics that precisely counteracts the prescribed large-scale forcing in order to maintain the steady state.
- Since the LES results indeed succeed in maintaining the stationary state such as observed, the additional advantage of long time averaging is allowed, which improves the output statistics.
- The BOMEX case, such as described in [43] has been subjected to an intercomparison of 11 LES codes [46]. Since the report of this intercomparison is in progress, here we show only results from the LES model used in [43]. However, it should be realized that all the main features we discuss in this section are supported by other LES codes.

5.2. CASE DESCRIPTION AND GENERAL RESULTS

In [43] a large-eddy simulation has been described based on observations during the undisturbed period of BOMEX. During this period, non-precipitating clouds were the only type of cumuli that were observed under steady state conditions. Initial profiles of the specific humidity q_v and the potential temperature θ are shown in Fig. 12 along with observations. Note the typical shape of the profiles, consisting of a well-mixed convective subcloud layer, a conditionally unstable cloud layer topped by a strong inversion.

The large-scale forcing, dominated by subsidence, is prescribed using results of budget studies from BOMEX [19, 43]. This subsidence causes strong drying and heating, especially in the inversion layer. Since this is a case with a low cloud cover it is not necessary to use an interactive radiation scheme but instead a clear sky radiative cooling is prescribed.

Using the prescribed large-scale forcings and the initial profiles as described above, an LES run of 7 hours has been performed. Figure 12 shows the initial profiles and the mean profiles of θ and q_v after 3 and 7 hours of simulation. From this we can see that the model is in a steady-state, in agreement with observations.

This implies that the latent heat surface flux (about 150 W/m^2 in this case) has to be distributed by turbulent transport so as to counteract the large-scale drying by subsidence. In order to gain some insight in how this is achieved we show in Fig. 13 the various terms of the budget equations for q_v and q_ℓ

$$\frac{\partial \overline{q_v}}{\partial t} = -\frac{\partial \overline{w' q_v'}}{\partial z} - (c - e) + \left(\frac{\partial \overline{q_v}}{\partial t}\right)_{\text{forcing}},$$

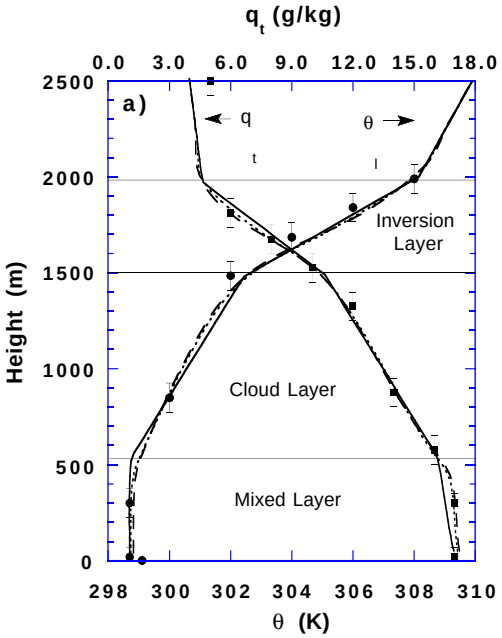

Figure 12. Horizontally averaged profiles of θ and q_v at times t=0 hr, (full lines) t=3hr (dotted lines) and t=7hr (dashed lines). The circles and squares are the observed values.

$$\frac{\partial \overline{q_\ell}}{\partial t} = -\frac{\partial \overline{w' q'_\ell}}{\partial z} + (c - e) + \left(\frac{\partial \overline{q_\ell}}{\partial t}\right)_{\text{forcing}}, \tag{35}$$

as determined by the LES model. The bars indicate an area average over the horizontal domain of the model. The large-scale advection and subsidence terms have been collected in one forcing term (*cf.* (33)). In order to improve the statistics, all terms in (35) are averaged over the last 4 hours of the simulation.

For liquid water we observe a strong positive condensation near cloud base around 500m, which is balanced by turbulent transport; the generated liquid water is transported upward, riding on its own generated buoyancy. Near the inversion where the clouds loose their buoyancy the upward transported liquid water is evaporated back into the water vapor. So after all is said and done there is no net liquid water production. The liquid water is only a temporary disguise of the moisture to generate the necessary buoyancy in order to penetrate through the conditionally unstable layer into the inversion layer and to deposit air from subcloud layer there. From the q_v budget we see that the liquid water is not the only moisture that is

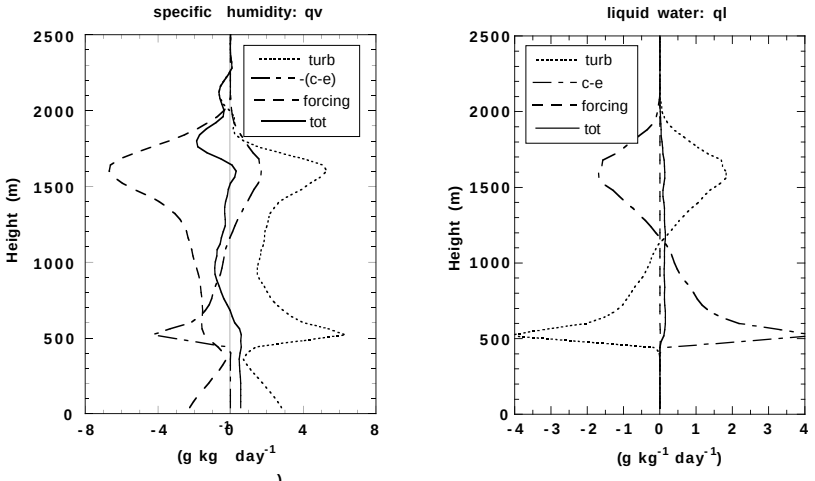

Figure 13. The various terms from the q_ℓ (left panel) and the q_v (right panel) budget equation (35) integrated over the last 4 hrs of simulation. Terms are as follows: turb = turbulent flux divergence, c-e = condensation minus evaporation, forcing = large-scale forcing and tot: total tendency as a result of all processes.

transported. Since the air is saturated in the buoyant cloud channels, most of the moisture transport is through the water vapor.

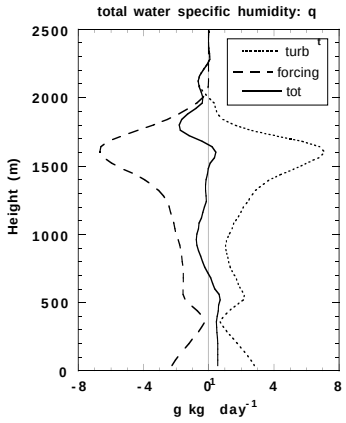

Figure 14. As Fig. 13 but now for the q_t budget equation (36).

The total moisture transport can be easily summarized by considering the sum of the two budget equations (35)

$$\frac{\partial \overline{q_t}}{\partial t} = -\frac{\partial \overline{w' q_t'}}{\partial z} + \left(\frac{\partial \overline{q_t}}{\partial t}\right)_{\text{forcing}}. \tag{36}$$

Since the condensation term has dropped out we can now directly observe (see Fig. 14) a balance between the large-scale forcing and the moisture transport due to the cumulus convection. For a similar discussion on the heat budget equation we refer to Siebesma and Cuijpers [43].

5.3. CLOUD COVER AND MASS FLUX

Figure 15 shows a snapshot of the 3-D cloud field generated by the LES model. A striking feature is that clouds vary significantly in size. In fact only very few clouds actually do reach the inversion. This is illustrated more quantitatively in Fig. 16a where the fractional cloud cover a_c (see Appendix A for a precise definition) is shown as a function of height.

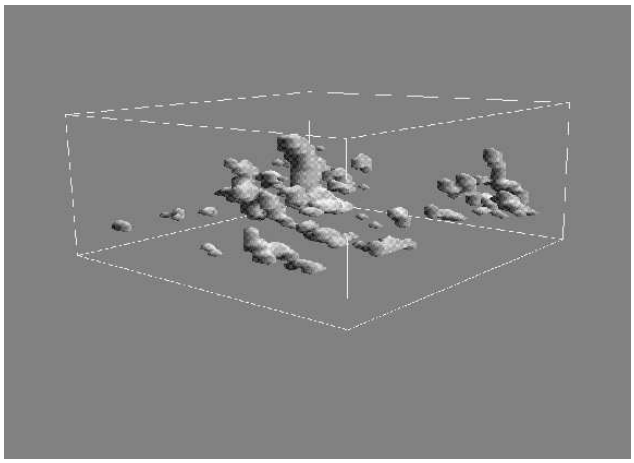

Figure 15. Snapshot of the 3-D cloud field generated by the LES model

A strong systematic decrease of a_c with height is apparent. Figure 16a also shows the part of the cloud fraction due to updrafts and downdrafts. From this we conclude that cloud downdrafts play only a minor role. Finally, the cloud core cover, defined as the fraction of cloudy grid points that are positively buoyant, is shown in Fig. 16a. Note that 50 % of the cloudy grid points are positively buoyant. The remaining part is either passive or forced.

The vertical mass transport through the cloud ensemble is measured by the mass flux which is defined as $M \equiv \rho a_c w_c$. Setting ρ equal to 1 for simplicity, it is essentially the product of the cloud cover a_c and the vertical velocity w_c of the cloud ensemble. The mass flux is an important quantity, since in many cumulus parameterizations, the turbulent flux of a field ϕ is estimated using the so-called mass flux approximation

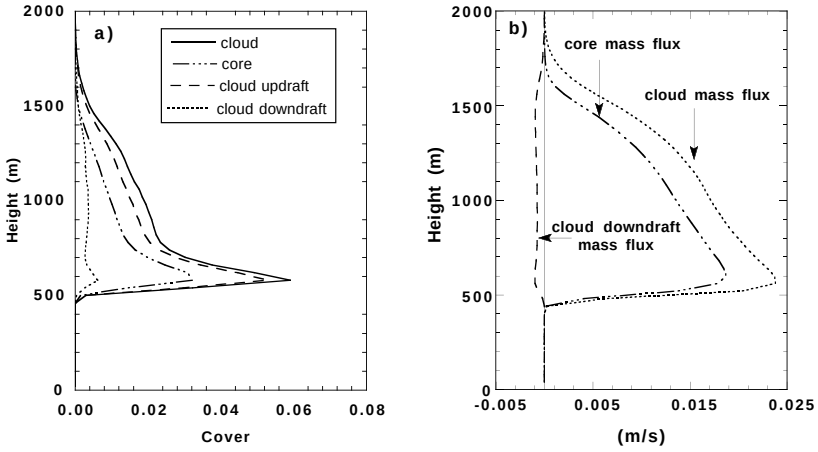

Figure 16. Fractional cover (a) and mass flux (b) of: clouds, cloud updrafts, cloud downdrafts and the cloud core as a function of height. See text for further discussion

$$\overline{w'\phi'} \approx M(\phi_c - \phi_e). \tag{37}$$

In Fig. 16b we show the mass flux for the whole cloud ensemble, the cloud core and the updrafts and downdrafts within the clouds. A few important conclusions can be drawn:

- There is a systematic decrease of the mass flux with height, which is due to the decrease of the cloud cover with height.
- Mass downdrafts in the clouds are unimportant. Apparently, penetrative evaporatively driven downdrafts are not present *within* the clouds.
- Most of the vertical mass transport is carried by the core of the clouds.

5.4. CONDITIONALLY SAMPLED THERMODYNAMIC FIELDS

We saw in section 3 that the in-cloud values of $q_{t,c}$ and $\theta_{l,c}$ are only constant with height, if clouds do *not* mix with the environment. In Fig. 17 we show the conditionally sampled cloud and core fields of q_t and θ_ℓ. The effect of mixing with the environment is clearly visible. Note that the cloud fields are now representing the whole cloud ensemble (see Appendix A for precise definitions) rather than individual clouds as in section 3. From Fig. 17 we can also conclude that the core has mixed less intensively with the environment than the whole cloud ensemble. This is due to the fact that the core points are mostly in the center of the clouds and are effectively shielded from the environment.

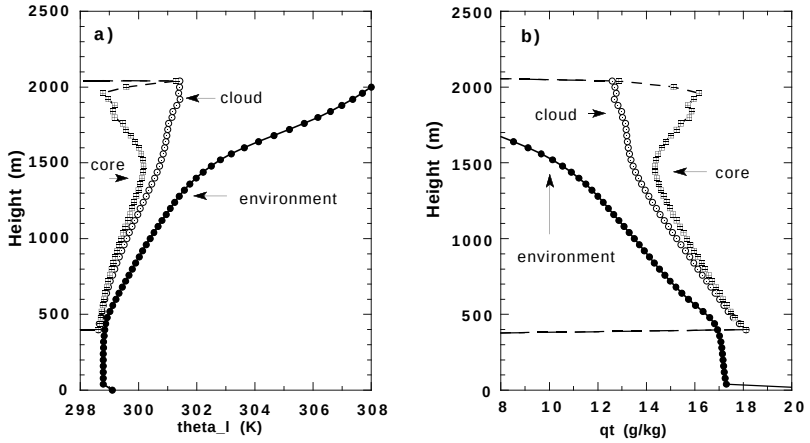

Figure 17. Conditionally sampled cloud and core fields of q_t and θ_ℓ along with the environmental profiles.

In Fig. 18 we show the environmental virtual potential temperature $\overline{\theta_v}$ along with the values of $\theta_{v,c}$ in the clouds and in the core. We find the rather striking result that the cloud ensemble is almost neutrally buoyant with respect to the environment in the cloud layer, while the core is only marginally positively buoyant with a virtual temperature excess of only a few tenths of a degree. Apparently, in the present shallow cumulus case there is only a small potential barrier, *i.e.* little negative CAPE between LCL and the LFC. Hence, there is little chance to build up CAPE, because it is almost directly consumed by the clouds and transferred into kinetic energy, thereby maintaining an almost neutrally buoyant state. This situation has to be contrasted with deep convection where a considerable CAPE can build up that is subsequently released in more violent and precipitating deep convective events. In this sense deep convection is more episodic than shallow cumulus convection.

5.5. ENTRAINMENT OF THE CUMULUS ENSEMBLE

In the previous section we saw how the temperature and moisture of the cloud ensemble are affected by entrainment. In order to quantify the entrainment we assume that the same lateral entrainment arguments for a single cloud (see section 3.2) can now be applied to a cloud *ensemble*. In that case equation (27) can be used and written as

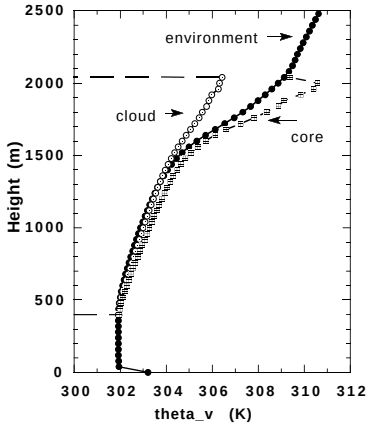

Figure 18. As in Fig. 17 but for θ_v.

$$\varepsilon = -\frac{\partial \phi_c / \partial z}{(\phi_c - \phi_e)}, \tag{38}$$

where the fractional entrainment rate ε should now be interpreted as representative of a whole cloud ensemble. Using the conditionally sampled fields we can therefore determine the fractional entrainment. Results are shown in Fig. 19 for the cloud ensemble (left panel) and the core ensemble (right panel). Each calculation is done for both $\phi = q_t$ and $\phi = \theta_\ell$. From this we can draw the following conclusions:

- We find a typical value of $\varepsilon \approx 3 \times 10^{-3}$ m^{-1} in agreement with the order of magnitude estimate (29).
- This value is much higher than the classic plume result (30): Using a typical cloud radius of 500 m in (30) gives $\varepsilon \approx 2 \times 10^{-4}$ m^{-1}, a factor of 10 smaller than the present LES results.
- As already noted in the previous section, entrainment in the core is systematically smaller than in the clouds.
- Above the cloud base we observe a systematic decrease of ε with height. This can be interpreted as evidence for (28). Assuming that mixing at height z is dominated by those cloud members of the ensemble that actually do reach that height (see Fig. 20), we find, using (28), for the fractional entrainment rate ε of the whole cloud ensemble

$$\varepsilon \sim \frac{1}{z - z_{lcl}}. \tag{39}$$

- Since ε is a purely turbulent mixing parameter, it should only depend on the velocity field. This implies that equation (38) should give the

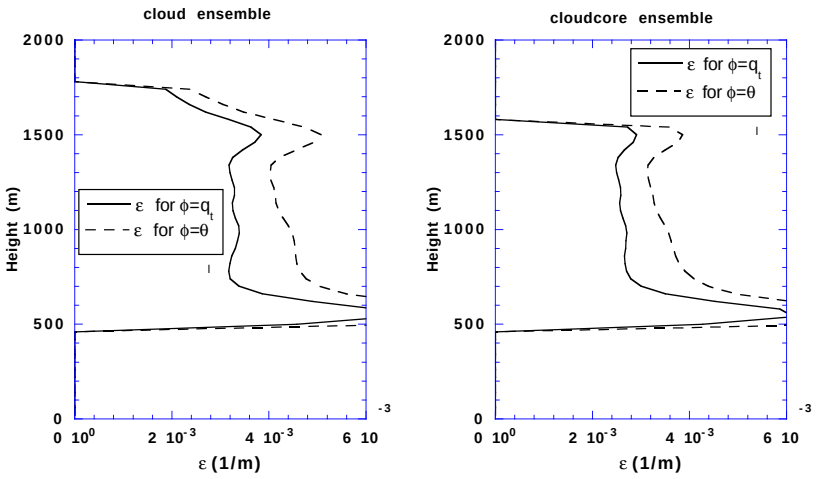

Figure 19. Fractional entrainment rate ε using (38) based on $\phi = \{\theta_\ell, q_t\}$ for both the cloud ensemble (left panel) and the core (right panel).

same results for q_t and θ_ℓ. This is true only approximately (see Fig. 19). Clearly, this is due to one or more of the numerous assumptions that went into (38). This point will be further investigated in the next section.

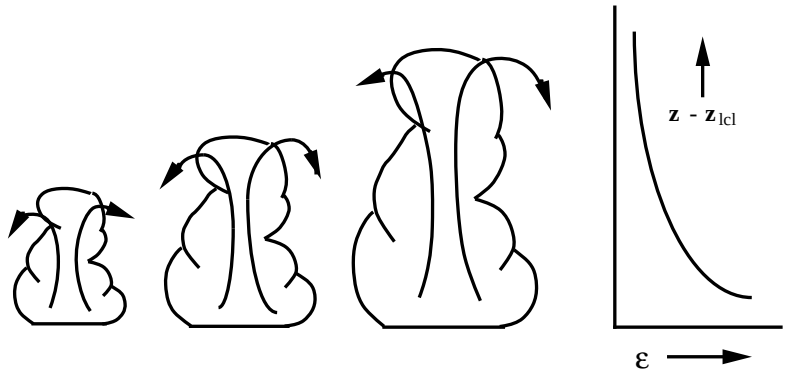

Figure 20. Schematic illustration of the arguments leading to (39). The most active eddies with respect to the turbulent mixing between clouds and the environment at height z are those eddies formed by clouds that actually do reach that height.

6. Parameterizations of Entrainment and Detrainment

6.1. INTRODUCTION

So far, entrainment has been used as a rather vague mixing concept. In fact the only quantitative result, (38), is based on hand-waving arguments. Also in the literature, the concepts of entrainment and detrainment often remain rather descriptive. Therefore, we will start in section 6.2 with precise definitions of entrainment and detrainment. The objective is then to invoke these definitions in separate budget equations for the cloudy part and the environmental part and determine the lateral mass exchange between these regions as residuals. However, in order to do so we have to make a mean field approximation for the lateral mass exchange and test its validity with LES (see section 6.3). Further simplifications made in section 6.4 lead finally to a mass flux parameterization for shallow cumulus. The most important free parameters in this parameterization are precisely the entrainment and detrainment rates. Typical values will be determined from LES. Ideally one would like to have a dynamical parameterization for these rates. An attempt in this direction is finally presented in section 6.5.

We saw in section 5.3 that most of the vertical transport takes place in the core of the clouds. Therefore to remain concrete, from now on the subscripts c and e should be interpreted as the core part and its complementary part. However, it should also be understood that the arguments hold for any arbitrary interface, so the derived equations can also be used for a cloud interface or, in case of the dry convective boundary layer, for an updraft-downdraft interface.

6.2. DEFINITIONS OF ENTRAINMENT AND DETRAINMENT

In Appendix A we derived the spatially averaged continuity equation for the cloudy region

$$\frac{\partial a_c}{\partial t} + \frac{1}{A}\oint_{\text{interface}} \hat{\mathbf{n}} \cdot (\mathbf{u} - \mathbf{u_i}) dl + \frac{\partial a_c w_c}{\partial z} = 0, \tag{40}$$

where $a_c = A_c/A$ is the fractional cloud cover, $\hat{\mathbf{n}}$ is a unit vector perpendicular to the interface, $\mathbf{u}$ is the full 3D velocity vector of the mass flow at the interface and $\mathbf{u_i}$ is the velocity of the interface. In mass flux parameterizations [2] the entrainment and detrainment rates E and D are usually introduced as

$$\frac{\partial a_c}{\partial t} + (D - E) + \frac{\partial a_c w_c}{\partial z} = 0. \tag{41}$$

Comparing (40) and (41) shows that $D - E$ can be defined as

$$D - E \equiv \frac{1}{A}\oint_{\text{interface}} \hat{\mathbf{n}} \cdot (\mathbf{u} - \mathbf{u_i}) dl, \tag{42}$$

which clearly defines $D - E$ as the net mass exchange across the interface. Let us emphasize that it is the mass velocity $\mathbf{u}$ *relative* to the interface velocity $\mathbf{u_i}$ that enters the definition (42). This way it is guaranteed that $D - E = 0$ if a cloud is simply advected by the mean wind.

Since entrainment deals with inflow and detrainment with outflow we proceed by postulating separate definitions for E and D

$$\begin{aligned} E &= -\frac{1}{A}\oint_{\hat{\mathbf{n}}\cdot(\mathbf{u}-\mathbf{u_i})<0} \hat{\mathbf{n}}\cdot(\mathbf{u}-\mathbf{u_i})dl, \\ D &= \frac{1}{A}\oint_{\hat{\mathbf{n}}\cdot(\mathbf{u}-\mathbf{u_i})>0} \hat{\mathbf{n}}\cdot(\mathbf{u}-\mathbf{u_i})dl, \end{aligned} \tag{43}$$

so that entrainment is just defined as that part of the contour integral (42) where there is an inflow of mass into the cloudy part and detrainment as the complementary part where there is mass outflow into the environment (see Fig. 21).

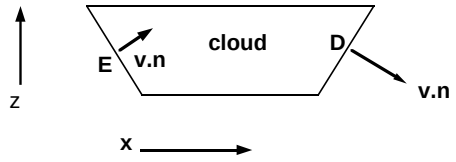

Figure 21. Entrainment is the inflow of mass and detrainment outflow of mass across the interface.

6.3. MEAN FIELD APPROXIMATIONS

Matters become complicated more if we want to employ E and D, as defined in (43), in the budget equations of an arbitrary field ϕ for the core and its complementary, environmental part, (see Appendix A for a derivation),

$$\begin{aligned} \frac{\partial a_c\phi_c}{\partial t} &= -\frac{\partial a_c\overline{w\phi}^c}{\partial z} - \frac{1}{A}\oint_{\text{interface}} \hat{\mathbf{n}}\cdot(\mathbf{u}-\mathbf{u_i})\phi dl + a_c F_c, \\ \frac{\partial\left(1-a_c\right)\phi_e}{\partial t} &= -\frac{\partial\left(1-a_c\right)\overline{w\phi}^e}{\partial z} + \frac{1}{A}\oint_{\text{interface}} \hat{\mathbf{n}}\cdot(\mathbf{u}-\mathbf{u_i})\phi dl + \left(1-a_c\right)F_e, \end{aligned} \tag{44}$$

where all possible sinks and sources are absorbed in the forcing term F. At this point it is impossible to infer E and D as defined in (43). In order to obtain budget equations useful for parameterizations we make the mean field

approximation that entrainment transports *average* environmental properties into the core and, vice versa, *average* core properties are detrained into the environment, (see Fig. 22),

$$\begin{aligned} E_\phi \phi_e &\simeq -\frac{1}{A} \oint_{\hat{\mathbf{n}}\cdot(\mathbf{u}-\mathbf{u_i})<0} \hat{\mathbf{n}} \cdot (\mathbf{u}-\mathbf{u_i}) \phi dl, \\ D_\phi \phi_c &\simeq \frac{1}{A} \oint_{\hat{\mathbf{n}}\cdot(\mathbf{u}-\mathbf{u_i})>0} \hat{\mathbf{n}} \cdot (\mathbf{u}-\mathbf{u_i}) \phi dl. \end{aligned} \tag{45}$$

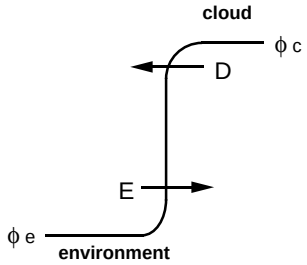

Figure 22. The mean field approximation (45) assumes a top-hat distribution for the field ϕ : the average environmental field ϕ_e is entrained into the clouds and the average cloud field ϕ_c is detrained into the environment.

We have indexed the "effective medium" exchange rates E_ϕ and D_ϕ to indicate that there might be a ϕ dependence. Let us stress however that (45) is a useful approximation only if $E_\phi = E$ and $D_\phi = D$. Accepting this strong assumption for the moment we can use (45) in (44):

$$\begin{aligned} \frac{\partial a_c \phi_c}{\partial t} &= E\phi_e - D\phi_c - \frac{\partial a_c \overline{w\phi}^c}{\partial z} + a_c F_c, \\ \frac{\partial (1-a_c)\phi_e}{\partial t} &= -E\phi_e + D\phi_c - \frac{\partial (1-a_c)\overline{w\phi}^e}{\partial z} + (1-a_c) F_e. \end{aligned} \tag{46}$$

The validity of the assumption (45) has been tested using LES results for BOMEX by calculating E and D as residuals of (46) for different fields $\phi = \{\theta_\ell, q_t\}$ [46]. The results, displayed in Fig. 23, do not show any ϕ-dependence. Although this is not a complete proof for $E = E_\phi$ and $D = D_\phi$, it does show that (46) gives consistent results so that we can indeed use these equations to investigate mixing between core and the environment.

Before we proceed with simplifying (46) even more to derive suitable parameterizations let us pause for a moment and ask the question whether

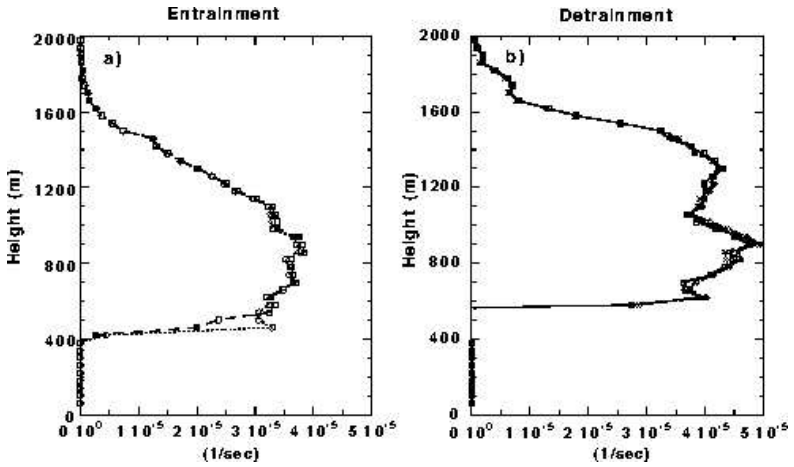

Figure 23. Entrainment and detrainment rates determined using LES data for different fields. In a) entrainment rates are obtained as a residual of (46) for $\phi = q_t$ (squares) and $\phi = \theta_\ell$ (circles). In b) as in a) but for detrainment. In b) we also plot the detrainment rate computed as a residual of the continuity equation (41). Note an extraordinary data collapse for all calculations.

assumption (45) already excludes stochastic mixing mechanisms such as introduced in section 3.6. In other words, do we already make a choice for lateral mixing when taking (46) as a starting point for parameterizations? The answer is partly yes since (46) assumes a top-hat distribution for the mixing between clouds and the environment, similar to the assumption that led to the lateral mixing result (27). On the other hand, by keeping the third term on the rhs of (46), there is still a freedom for variability of the fields within the cloudy and environmental regions. Therefore, by accepting (46), we are halfway to a lateral mixing model.

6.4. MASS FLUX PARAMETERIZATION WITH LATERAL MIXING

In order to formulate a practical parameterization for large-scale models, further simplifications of (46) are necessary. We therefore make three approximations:

- the mass flux approximation $\overline{w\phi}^c \simeq w_c \phi_c$,
- the core cover is much smaller than 1, *i.e.* $a_c \ll 1$, so that $\phi_e \approx \overline{\phi}$,
- steady state for the cloud ensemble $\partial a_c \phi_c / \partial t = 0$,

so that (41) and (46) can be simplified to

$$\frac{\partial M}{\partial z} = E - D, \tag{47}$$

$$\frac{\partial M\phi_c}{\partial z} = E\overline{\phi} - D\phi_c, \tag{48}$$

$$\frac{\partial \overline{\phi}}{\partial t} = -\frac{\partial M\left(\phi_c - \overline{\phi}\right)}{\partial z} + \overline{F}. \tag{49}$$

where $M = a_c w_c$. This set of equations is essentially the mass flux parameterization for cumulus convection as proposed by Tiedtke [61] .The first term on the rhs of (49) is precisely the turbulent flux divergence within the mass flux approximation (37) that needs to be parameterized. Hence, the parameterization is reduced to the determination of M and ϕ_c. These can be obtained from the steady state cloud model, as defined by (47) and (48), *provided* we know E and D plus the boundary conditions of M and ϕ_c at the cloud base. The latter, also known as the closure problem, is an interesting and important topic in itself but is outside the scope of the present paper. The entrainment and detrainment rates are usually parameterized in terms of the mass flux

$$E = \varepsilon M, \qquad D = \delta M, \tag{50}$$

where fractional entrainment and detrainment rates ε and δ are introduced. Within the present framework it is easy to show that ε as defined in (50) coincides with the one introduced in (27) and used in (38).

In most parameterization ε and δ are prescribed as constants with typical values $\varepsilon, \delta \sim 10^{-4}\mathrm{m}^{-1}$ [1, 16, 61], based on (30). Using LES output for BOMEX, typical values for the exchange rates have been determined [43]

$$\begin{aligned} \varepsilon &\approx 1.5 \sim 2.5 \times 10^{-3}\ \mathrm{m}^{-1}, \\ \delta &\approx 2.5 \sim 3\ \times 10^{-3}\ \mathrm{m}^{-1}, \end{aligned} \tag{51}$$

The spread in the results in (51) is mainly due to variation of the rates with height. Various sensitivity tests have been made by varying the resolution and domain size of the LES model. In all cases the fractional entrainment and detrainment rates remained within the range indicated by (51). Note that these values appear to be almost one order of magnitude larger than values suggested by (30) and used in many cumulus parameterizations. Furthermore, note that the detrainment is systematically larger than the entrainment consistent with the monotonic decrease of the mass flux with height (see section 5.3).

One may wonder how typical the results in (51) are for shallow convection in general. Recently we have made LES runs based of a North Sea cumulus case, as defined in [50] and of the Puerto Rico case, as defined in [11]. In both cases we found typical values in the range indicated by (51).

The parameterization (47-49) has been evaluated analytically for BOMEX [44] using constant prescribed values of ε and δ as suggested by the

LES results (51). The resulting turbulent fluxes and cloud fields compared well with the LES results indicating that the mass flux parameterization (47)-(49) is a sound approach *provided* the correct values for ε and δ are used.

We do not claim that the numerical values of ε and δ in (51) are universal. They are likely a function of the environmental conditions and will change from case to case. What is needed is a dynamical parameterization for these exchange rates based on physical concepts rather than using prescribed values. An attempt at that is made in the next subsection.

6.5. PARAMETERIZATION FOR ENTRAINMENT AND DETRAINMENT

Making similar approximations as in the last subsection, we can write the vertical momentum equation of the cloudcore region as [48, 46]

$$B - \varepsilon w_c^2 - w_c \frac{\partial w_c}{\partial z} = 0, \tag{52}$$

where the buoyancy B is given by

$$B = g \frac{\left(\theta_{v,c} - \overline{\theta}_v\right)}{\overline{\theta}_v}. \tag{53}$$

Equation (52) is a well-known and useful result since it relates the fractional entrainment to the buoyancy B and the vertical cloudcore velocity w_c. However, since w_c is an extra unknown variable it does not provide a solution for ε directly. We therefore consider the continuity equation (47) using (50) to arrive at

$$\frac{1}{a_c}\frac{\partial a_c}{\partial z} + \frac{1}{w_c}\frac{\partial w_c}{\partial z} = \varepsilon - \delta. \tag{54}$$

A proposal of Nordeng [37] is to link δ to the core cover divergence since detrainment is closely related to the evaporation of clouds. The remaining ε is then coupled to the vertical velocity divergence. This way one obtains two equations out of (54)

$$\frac{1}{w_c}\frac{\partial w_c}{\partial z} = \varepsilon, \tag{55}$$

$$\frac{1}{a_c}\frac{\partial a_c}{\partial z} = -\delta. \tag{56}$$

Combining (55) with (52) and integrating the vertical velocity from cloud base z_{lcl} to an arbitrary height z provides a parameterization for the fractional entrainment ε only in terms of buoyancy $B(z)$ and the cloudcore base

vertical velocity

$$\varepsilon(z) = \frac{B(z)}{2\left[w_c^2(z_{lcl}) + \int_{z_{lcl}}^{z} B(z)dz\right]}. \tag{57}$$

Note that this parameterization has the same scaling behavior as (39) if $B(z)$ is height independent.

Given the boundary conditions, *i.e.* the cloud fields at the cloud base, this provides a closed set of equations; the cloud model (47-48) provides $B(z)$ if ε is known and, vice versa, (57) provides $\varepsilon(z)$ if $B(z)$ is known. Therefore all cloudcore fields ϕ_c, the buoyancy B and ε can be solved iteratively.

The final free parameter that remains to be determined is the fractional detrainment δ in order to determine the mass flux from (47). Since it seems that a typical feature of shallow cumulus convection is that the mass flux decreases monotonically with heigth, the simplest way to assure this is to parameterise the fractional detrainment rate δ as

$$\delta = \varepsilon \frac{1}{z_{lnb} - z} \qquad\qquad z_{lcl} \leq z \leq z_{lnb} \tag{58}$$

where z_{lnb} is the neutral buoyancy level, that is used as an estimate of the highest cloud top.

Tests with a one-column version of the ECMWF model with the entrainment/detrainment parameterization (57-58) in conjunction with the mass flux parameterization (47-49) has given promising results [45].

7. Conclusions and Perspectives

This paper has reviewed our current understanding of shallow cumulus convection with emphasis on the mixing between cumulus clouds and their environment. Entrainment of dry air into cumulus clouds and detrainment of cloudy air into the environment affects significantly the dynamics and their interaction with the environment. It determines where in the cloud layer the ventilated heat and moisture from the subcloud layer will be deposited.

The main controversy in the field is whether this mixing can be described by a relative simple lateral mixing principle, or whether one has to resort to the more elaborate buoyancy sorting models. Essential in the latter mechanism is that mixing of clouds with the environment takes place in discrete events whereafter both ascending positively buoyant and descending negatively buoyant cloud parcels are all en route to their zero buoyancy level where they finally detrain by evaporation.

As discussed in section 3.5, it is difficult to draw conclusions on the basis of conserved variable diagrams only. Recent observations of kinematics [25,

40], LES results [43] and 2-D CRM results [30] seem to suggest that cloud downdrafts, although present, do not play a dominant role in the dynamics of shallow cumulus clouds. This supports the picture of an intermittant rising thermal, existing of an ensemble of rising mixtures, as schematically sketched in Fig. 9. Such a model does not suffer from the Warner paradox [66] since the cloud top is determined by the most buoyant undiluted parcels while other parcels dilute the cloud sufficiently by lateral entrainment. This intermittant entraining thermal model is somewhat in the middle between the classic plume model and the more trendy episodic buoyancy sorting models [13, 42].

In the light of this one may wonder why a simple mass flux parameterization [61] is so well capable in reproducing the shallow cumulus dynamics such as observed during BOMEX, provided it is feeded with the correct lateral entrainment rates [44]. Probably this is the case because the dynamics is mainly determined by the active core, *i.e.* the most buoyant part of the cloud ensemble. This way even a single entraining plume model of the core can overcome the Warner paradox as suggested also in [31]. Nevertheless, the possibility for a need of a description of *multiple* rising mixtures should not be excluded. Analysis of LES data using conserved variable diagrams should give further insight into this topic.

Another important related issue that has not been addressed in this paper deals with the question of how much air is entrained from the dry convective boundary layer into the cloud layer. This determines the boundary layer ventilation, boundary layer equilibrium and the surface evaporation. In General Circulation Models (GCM's) it is still common practice that turbulent transport in the subcloud layer and in the cloud layer are parameterized separately. This implies that for a shallow cumulus parameterization the turbulent fluxes at the cloud base need to be specified, which is called the closure problem. Usually this is solved by assuming a rather arbitrary coupling on the latent heat flux at the surface [61] or by relating it to CAPE [16, 37]. The dry convective boundary layer parameterization scheme [20, 32], on the other hand, has entrainment at the top with no knowledge of the existence of clouds, which leads to possible overlaps between the schemes and double counting of transport mechanisms [34]. A physical coupling between the turbulent transport in the cloud and dry convective boundary layer and its parameterization needs to be established. It is clear that the boundary layer ventilation is determined by the strongest thermals in the subcloud layer that condensate at the lifting condensation level (LCL) and have enough kinetic energy to reach the level of free convection (LFC). An investigation of the dynamics of such strong updrafts in the dry convective boundary layer can be regarded as a first preliminary step in this direction [64].

8. Acknowledgements

I would like to thank Aad van Ulden for interesting discussions and suggestions and Harm Jonker for a critical reading of the manuscript. Special thanks are given to Vanda Grubišić for a careful and constructive review of the paper.

Appendix A: Budget Equations for Conditionally Sampled Fields

8.1. DEFINITIONS AND AVERAGING PROCEDURES

Consider an arbitrary field ϕ in a domain with an horizontal area A. We denote a horizontal spatial average of this field with an overbar

$$\overline{\phi}(z) \equiv \frac{1}{A}\int_0^{L_x}\int_0^{L_y}\phi(x,y,z)dxdy \quad \text{with} \quad A = L_xL_y. \tag{59}$$

Within this domain there exist possibly nonconnected cloudy parts that vary in time and space. We define cloud and environment averages as spatial averages over the corresponding parts

$$\begin{aligned}\overline{\phi}^c = \phi_c &\equiv \frac{1}{A_c}\int\int_{\text{cloudy part}}\phi dxdy,\\ \overline{\phi}^e = \phi_e &\equiv \frac{1}{A_e}\int\int_{\text{env part}}\phi dxdy,\end{aligned} \tag{60}$$

where A_c and A_e denote the area over the cloudy and the environmental part. Clearly, ϕ_c and ϕ_e are trivially related

$$\overline{\phi} = a_c\phi_c + (1-a_c)\phi_e, \tag{61}$$

where $a_c = A_c/A$ is the fractional cloud cover. The vertical turbulent flux of ϕ is defined as

$$\overline{w'\phi'} \equiv \overline{w\phi} - \overline{w}\,\overline{\phi}. \tag{62}$$

Likewise we can define turbulent fluxes within the cloudy and environmental part

$$\begin{aligned}\overline{w'\phi'}^c &\equiv \overline{w\phi}^c - w_c\phi_c,\\ \overline{w'\phi'}^e &\equiv \overline{w\phi}^e - w_e\phi_e.\end{aligned} \tag{63}$$

Again the cloudy and environment fluxes are related

$$\overline{w'\phi'} = a_c\overline{w'\phi'}^c + (1-a_c)\overline{w'\phi'}^e + a_c(w_c - \overline{w})(\phi_c - \phi_e). \tag{64}$$

We will also need the average field ϕ_b and the turbulent flux at the cloud boundary

$$\overline{\phi}^b = \phi_b \equiv \frac{1}{L_b}\int_{\text{cloud interface}} \phi dl,$$
$$\overline{w'\phi'}^b \equiv \overline{w\phi}^b - w_b\phi_b, \tag{65}$$

where L_b denotes the total length of the cloud boundary.

BUDGET EQUATIONS

The prognostic equation for ϕ for a nondivergent velocity field can be written as

$$\frac{\partial\phi}{\partial t} + \nabla_h \cdot \mathbf{v}\phi + \frac{\partial w\phi}{\partial z} = F, \tag{66}$$

where $\mathbf{v}$ denotes the horizontal part of the velocity vector and w its vertical component. For the sake of simplicity we shall assume constant density but the equations can be easily generalized for the quasi-Boussinesq approximation. All possible source and sink terms are collected in F. The objective is to integrate all the terms of (66) over a horizontal cloudy area $A_c(z,t)$. Applying the Leibnitz theorem on the first and third term of the lhs of (66),

$$\frac{1}{A}\int_{A_c(z,t)} \frac{\partial\phi}{\partial t} dxdy = \frac{\partial a_c\phi_c}{\partial t} - \phi_b\frac{\partial a_c}{\partial t},$$
$$\frac{1}{A}\int_{A_c(z,t)} \frac{\partial w\phi}{\partial z} dxdy = \frac{\partial a_c\overline{w\phi}^c}{\partial z} - \overline{w\phi}^b\frac{\partial a_c}{\partial z}, \tag{67}$$

we find

$$\frac{\partial a_c\phi_c}{\partial t} - \phi_b\frac{\partial a_c}{\partial t} + a_c\overline{\nabla_h \cdot \mathbf{v}\phi}^c - \overline{w\phi}^b\frac{\partial a_c}{\partial z} + \frac{\partial a_c\overline{w\phi}^c}{\partial z} = a_cF_c. \tag{68}$$

For $\phi = 1$ and $F_c = 0$ we recover the continuity equation

$$\frac{\partial a_c}{\partial t} - \frac{\partial a_c}{\partial t} + a_c\overline{\nabla_h \cdot \mathbf{v}}^c - w_b\frac{\partial a_c}{\partial z} + \frac{\partial a_cw_c}{\partial z} = 0, \tag{69}$$

which can be put in a more transparent form by applying the divergence theorem

$$\frac{\partial a_c}{\partial t} + \frac{1}{A}\oint_{\text{interface}} \hat{\mathbf{n}} \cdot (\mathbf{u} - \mathbf{u_i})dl + \frac{\partial a_cw_c}{\partial z} = 0, \tag{70}$$

where $\hat{\mathbf{n}}$ is an outward pointed unit normal vector at the interface at height z, $\mathbf{u}$ is the full 3D vector of the (mass) velocity at the interface and $\mathbf{u_i}$

is the velocity of the interface itself. Note that the normal vector does not necessary point into the horizontal direction. Likewise, using the divergence theorem, (68) can be rewritten as

$$\frac{\partial a_c \phi_c}{\partial t} + \frac{1}{A} \oint_{\text{interface}} \hat{\mathbf{n}} \cdot (\mathbf{u} - \mathbf{u_i}) \phi dl + \frac{\partial a_c \overline{w\phi}^c}{\partial z} = a_c F_c. \tag{71}$$

Appendix B: List of Thermodynamic Constants

symbol	name	value
c_{pd}	specific heat capacity at constant pressure for dry air	1005 J kg^{-1} K^{-1}
c_{pv}	specific heat capacity at constant pressure for water vapor	1870 J kg^{-1} K^{-1}
c_l	specific heat capacity for liquid water	4190 J kg^{-1} K^{-1}
g	Acceleration due to gravity	9.81 m s^{-2}
L_0	Latent heat of vaporization at 273.15K	2.5 10^6 J kg^{-1}
p_0	reference pressure	1000 hPa
R_d	gas constant for dry air	287.05 J kg^{-1} K^{-1}
R_v	gas constant for water vapor	461.50 J kg^{-1} K^{-1}
ε	R_d/R_v	0.622
κ	R_d/c_{pd}	0.286

References

1. Anthes, R.A. (1977) A cumulus parameterization scheme utilizing a one-dimensional cloud model, *Mon. Wea. Rev.* **105**, 270-286.
2. Arakawa, A., and Schubert H. (1974) Interaction of a cumulus cloud ensemble with the large-scale environment. Part I. Theoretical formulation and sensitivity tests, *J. Atmos. Sci.* **31**, 674-701.
3. Augstein, E., Riehl H., Ostapoff F., and Wagner V. (1973) Mass and energy transports in an undisturbed trade-wind flow, *Mon. Wea. Rev.* **101**, 101-111.
4. Austin, P.H., Baker, M.B., Blyth, A.M. and Jensen, J.B. (1985) Small-scale variability in warm continental cumulus clouds, *J. Atmos. Sci.* **42**, 1123-1138.
5. Beniston, M.G., and Sommeria, G. (1981) Use of a detailed planetary boundary layer model for parameterization purposes, *J. Atmos. Sci.* **38**, 780-797.
6. Betts, A.K. (1973) Non-precipitating cumulus convection and its parameterization, *Quart. J. Roy. Meteor. Soc.* **99**, 178-196
7. Blyth, A.M., Cooper, W.A. and Jensen, J.B. (1988) A study of the source of entrained air in Montana cumuli, *J. Atmos. Sci.* **45**, 3944-3964.
8. Blyth, A.M. (1993) Entrainment in cumulus clouds, *J. App. Meteor.* **32**, 626-641.

9. Boatman, J.F. and Auer Jr., A.H. (1983) The role of cloud top entrainment in cumulus clouds, *J. Atmos. Sci.* **40**, 1517-1534.
10. Bougeault, Ph. (1981) Modeling the trade-wind cumulus boundary layer. Part I: Testing the ensemble cloud relations against numerical data, *J. Atmos. Sci.* **38**, 2414-2428.
11. Cuijpers, J.W.M, and Duynkerke, P.G. (1993) Large-eddy simulation of trade-wind cumulus clouds, *J. Atmos. Sci.* **50**, 3894-3908.
12. Deardorff, J.W., (1973) Three-Dimensional Numerical Modeling of the Planetary Boundary layer, in D.A Haugen (ed.), *Workshop on Micrometeorology*, Americ. Meteor. Soc., Boston, pp. 271-311.
13. Emanuel, K.A., (1991) A scheme for representing cumulus convection in large-scale models, *J. Atmos. Sci.* **48**, 2313-2335.
14. Emanuel, K.A., (1994) *Atmospheric Convection.* Oxford Univ. Press, Oxford.
15. Esbensen, S. (1978) Bulk thermodynamic effects and properties of small tropical cumuli, *J. Atmos. Sci.* **35**, 826-837.
16. Gregory, D. and Rowntree P. R. (1990) A mass flux scheme with representation of cloud ensemble characteristics and stability-dependent closure, *Mon. Wea. Rev.* **118**, 1483-1506.
17. Heymsfield, A.J., Johnson, P.N. and Dye, J.E. (1978) Observations of moist adiabatic ascent in northeast Colorado cumulus clouds, *J. Atmos. Sci.* **35**, 1689-1703.
18. Holland, J.Z., (1972) Comparative evaluation of some BOMEX measurements of sea surface evaporation, energy flux and stress, *J. Phys. Oceanogr.* **2**, 476-486.
19. Holland, J.Z., and Rasmusson, E.M. (1973) Measurement of atmospheric mass, energy and momentum budgets over a 500-kilometer square of tropical ocean. *Mon. Wea. Rev.* **101**, 44-55.
20. Holtslag, A.A.M. and Boville, B.A. (1993) Local versus nonlocal boundary-layer diffusion in a global climate model. *J. of Climate* 6, **6**, 1825-1842.
21. Hu, Q. (1997) A cumulus parameterization based on a cloud model of intermittently rising thermals, *J. Atmos. Sci.* **54**, 2292-2307.
22. Iribarne, J.V. and Godson, W.L. (1973) *Atmospheric Thermodynamics.* D. Reidel, Dordrecht.
23. Jensen, J.B., Austin P.H., Baker, M.B. and Blyth, A.M. (1985) Turbulent mixing, spectral evolution and dynamics in a warm cumulus cloud, *J. Atmos. Sci.* **42**, 173-192.
24. Johnson, R.H., and Lin, X. (1997) Episodic trade wind regimes over the western pacific warm pool, *J. Atmos. Sci.* **54**, 2020-2034.
25. Jonas, P.R. (1990) Observations of cumulus cloud entrainment, *Atmos. Res.* **25**, 105-107.
26. Kain, J.S. and Fritsch, J.M. (1990) A one-dimensional entraining/detraining plume model and its application in convective parameterization *J. Atmos. Sci.* **47**, 2784-2802.
27. Kain, J.S. and Fritsch, J.M. (1992) The role of the convective "trigger function" in numerical forecasts of mesoscale convective systems, *Meteorol. Atmos. Phys.* **49**, 93-106.
28. Klaassen, G.P., and Clark T.L. (1985) Dynamics of the cloud-environment interface and entrainment in small cumuli: Two-dimensional simulations in the absence of ambient shear. *J. Atmos. Sci.* **42**, 2621-2642.
29. Lamontagne, R.G., and Telford, J.W. (1983) Cloud top mixing in small cumuli, *J. Atmos. Sci.* **40**, 2148-2156.
30. Lin, C., and Arakawa, A. (1997) The macroscopic entrainment processes of simulated cumulus ensemble. Part I: Entrainment sources, *J. Atmos. Sci.* **54**, 1027-1043.
31. Lin, C., and Arakawa, A. (1997) The macroscopic entrainment processes of simulated cumulus ensemble. Part II: Testing the entraining plume model, *J. Atmos. Sci.* **54**, 1044-1053.
32. Louis, J-F., (1979) A parametric model of vertical eddy fluxes in the atmosphere, *Bound. Layer Meteor.* **17**, 187-202.
33. Nicholls, S., Lemone, M.A., and Sommeria, G. (1982) The simulation of a fair

weather marine boundary layer in GATE using a three-dimensional model, *Quart. J. Roy. Meteor. Soc.* **108**, 167-190.
34. Meijgaard, E. van (1996) Interaction of boundary-layer turbulence with shallow cumulus clouds over land. Proceedings on HIRLAM Workshop on Physical Parameterizations. Helsinki.
35. Nieuwstadt, F.T.M., (1998) Review of diffusion processes in the convective boundary layer. See this volume.
36. Nitta, T., and Esbensen, S. (1974) Heat and moisture budget analyses using BOMEX data, *Mon. Wea. Rev.* **102**, 17-28.
37. Nordeng, T.E. (1994) Extended versions of the convective parametrization scheme at ECMWF and their impact on the mean and transient activity of the model in tropics, Technical Memorandum No. 206, ECMWF, 41pp.
38. Paluch, I.R., (1979) The entrainment mechanism in Colorado cumuli, *J. Atmos. Sci.* **31**, 1028-1039.
39. Pontikis, C., Rigaud, A. and Hicks, E. (1987) Entrainment and mixing as related to the microphysical properties of shallow warm cumulus clouds, *J. Atmos. Sci.* **44**, 2150-2165.
40. Raga, G.B., Jensen, J.B., and Baker, M.B. (1990) Characteristics of cumulus band clouds off the coast of Hawaii, *J. Atmos. Sci.* **47**, 338-355.
41. Raymond, D.J., and Wilkening, M.H. (1982) Flow and mixing in New Mexico mountain cumuli, *J. Atmos. Sci.* **39**, 2211-2228.
42. Raymond, D.J., and Blyth, A.M. (1986) A stochastic model for nonprecipitating cumulus clouds, *J. Atmos. Sci.* **43**, 2708-2718.
43. Siebesma, A. P. and Cuijpers J. W. M. (1995) Evaluation of parametric assumptions for shallow cumulus convection, *J. Atmos. Sci.* **52**, 650-666.
44. Siebesma, A. P. and Holtslag A. A. M. (1996) Model impacts of entrainment and detrainment in shallow cumulus convection, *J. Atmos. Sci.* **53**, 2354-2364.
45. Siebesma, A.P. (1996) On the Mass Flux Approach for Atmospheric Convection. ECMWF Seminar Proceedings : New Insights and Approaches to Convective Parametrization. 34pp.
46. Siebesma, A.P., Brown, A., Cuxart, J., Sanchez, E., Moeng, C-H, Cotton, W.R., Jiang, H., Grubisic, V., Bretherton, C., Chlond, A., Khairoutdinov M., Krueger S., Lewellen, D., Macvean, M.K., Stevens, D. and Stevens, B. (1997) Intercomparison of 3d/2d cloud resolving models for the shallow-cumulus topped boundary layer, *In progress.*
47. Simpson, J., Simpson, R.H.D., Andrews, A. and Eaton, M.A. (1965) Experimental cumulus dynamics, *Rev. Geophys.* **3**, 387-431.
48. Simpson, J., and Wiggert, V. (1969) Models of precipitating cumulus towers, *Mon. Wea. Rev.* **97**, 471-489.
49. Simpson, J (1971) On cumulus entrainment and one-dimensional models, *J. Atmos. Sci.* **28**, 449-455.
50. Smith, S.A. and Jonas, P. (1995) Observations of the turbulent fluxes in fields of cumulus clouds, *Q. J. R. Meteorol. Soc.* **121**, 1185-1208.
51. Sommeria, G. (1976) Three-dimensional simulation of turbulent processes in an undisturbed trade-wind boundary layer, *J. Atmos. Sci.* **33**, 216-241.
52. Sommeria, G. and Lemone, M.A. (1978) Direct testing of a three-dimensional model of the planetary boundary layer against experimental data, *J. Atmos. Sci.* **35**, 25-39.
53. Squires, P. (1958) Penetrative downdraughts in cumuli, *Tellus* **10**, 381-389.
54. Squires, P. and J. S. Turner (1962) An entraining jet model for cumulonimbus updraughts, *Tellus* **14**, 422-434.
55. Stommel, H. (1947) Entrainment of air into a cumulus cloud, *J. Meteorol.* **4**, 91-94.
56. Stull, R.B. (1985) A fair-weather cumulus cloud classification for mixed-layer studies, *J. Clim. Appl. Meteorol.* **24**, 49-56.
57. Stull, R.B. (1988) *An Introduction to Boundary Layer Meteorology*, Kluwer Academic Publishers, 666pp.

58. Taylor, B.R. and Baker, M.B. (1991) Entrainment and detrainment in cumulus clouds, *J. Atmos. Sci.* **48**, 112-121.
59. Telford, J.W. (1975) Turbulence, entrainment and mixing in cloud dynamics, *Pure Appl Geophys.,* **113**, 1067-1084.
60. Tiedtke, M. (1987) The parametrization of moist processes. Part 2: The parametrization of cumulus convection. *ECMWF Lecture Series*, 56pp.
61. Tiedtke, M. (1989) A comprehensive mass flux scheme for cumulus parameterization in large-scale models, *Mon. Wea. Rev.* **177**, 1779-1800.
62. Tripoli, G.J. and Cotton, W.J. (1981) The use of ice-liquid water potential temperature as a thermodynamic variable in deep atmospheric models, *Mon. Weather Rev.* **109**, 1094-1102.
63. Turner, J.S. (1973) *Buoyancy effects in fluids* Cambridge University Press, 367 pp.
64. Van Ulden, A.P and Siebesma, A.P. (1997) A model for strong updrafts in the convective boundary layer, in Proceedings of: 12th Symposium on Boundary Layers and Turbulence, Vancouver, Canada, Americal Meteorological Society, 45 Beacon Street, Boston Massachusetts, MA02108-3693, USA. pp. 257-259.
65. Warner, J. (1955) The water content of cumuliform clouds, *Tellus* **7**, 449-457.
66. Warner, J. (1970) On steady-state one-dimensional models of cumulus convection, *J. Atmos. Sci.* **27**, 1035-1040.